



Deposited via The University of Leeds.

White Rose Research Online URL for this paper:

<https://eprints.whiterose.ac.uk/id/eprint/119515/>

Version: Accepted Version

---

**Article:**

Degardin, M, Thakar, D, Claron, M et al. (2017) Development of a selective cell capture and release assay: impact of clustered RGD ligands. *Journal of Materials Chemistry B*, 5 (24). pp. 4745-4753. ISSN: 2050-750X

<https://doi.org/10.1039/C7TB00630F>

---

© 2017, The Royal Society of Chemistry. This is an author produced version of a paper published in *Journal of Materials Chemistry B*. Uploaded in accordance with the publisher's self-archiving policy.

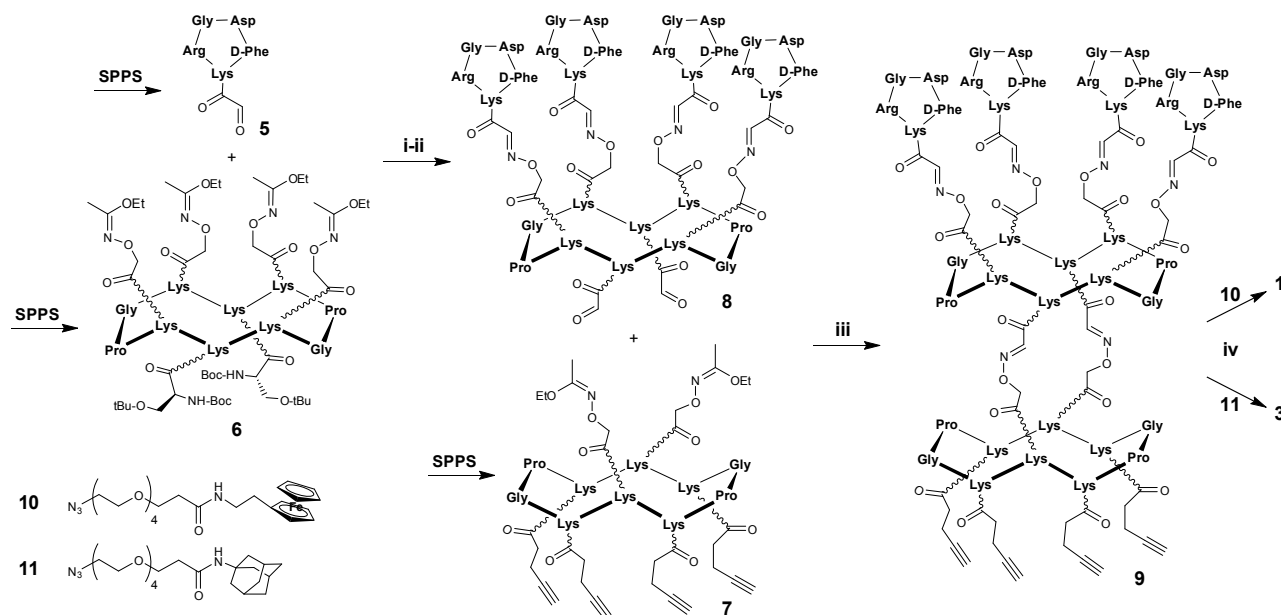
**Reuse**

Items deposited in White Rose Research Online are protected by copyright, with all rights reserved unless indicated otherwise. They may be downloaded and/or printed for private study, or other acts as permitted by national copyright laws. The publisher or other rights holders may allow further reproduction and re-use of the full text version. This is indicated by the licence information on the White Rose Research Online record for the item.

**Takedown**

If you consider content in White Rose Research Online to be in breach of UK law, please notify us by emailing [eprints@whiterose.ac.uk](mailto:eprints@whiterose.ac.uk) including the URL of the record and the reason for the withdrawal request.





**Scheme 1** Synthesis of compounds **1** and **3**. Reaction conditions: i) TFA/H<sub>2</sub>O (7:3), rt, 20 min then TFA/H<sub>2</sub>O (95:5), rt, 120 min, 44%; ii) NaIO<sub>4</sub>, H<sub>2</sub>O, rt, 20 min, 46%; iii) TFA/H<sub>2</sub>O/CH<sub>3</sub>CN (7:2:1), rt, 20 min, 42%; iv) CuSO<sub>4</sub>, THPTA, sodium ascorbate, phosphate buffer pH 7.4/DMF (6/4), 45°C, 150 min, **1**: 63%, **3**: 71%. SPPS: solid-phase peptide synthesis.

To date, the influence of individual RGD-containing molecules on cell adhesion, exhibiting monovalent vs. clustered ligands, has not been reported. To answer this question, we designed bifunctional compounds containing the cyclopentapeptide cell recognition motif RGD in either tetrameric (compound **1**) or monomeric presentation (compound **2**), and ferrocene (Fc) motifs for host-guest mediated attachment to surfaces with  $\beta$ -cyclodextrin ( $\beta$ -CD) functionalized self-assembled monolayers (SAMs) (Fig. 1). The use of supramolecular chemistry, particularly host-guest systems, is an attractive way to study cell-substrate interactions.<sup>11</sup> The redox properties of Fc have been exploited to provide reversible host-guest interactions. This property enables the cell capture and the release from the surface required for further cell analyses.<sup>12</sup> Herein, we report a new method for controlling the surface density of monomeric or tetrameric RGD compounds exploited for the selective  $\alpha_v\beta_3$ -expressing cell capture and release. Furthermore, a fundamental issue regarding the inter-ligand spacing for cell adhesion on surfaces was addressed.

## Results and discussion

As the affinity of Fc for  $\beta$ -CD is low ( $K_d = 250 \mu\text{M}$ ),<sup>13</sup> the macromolecules require multivalent interaction to strengthen

the binding of RGD bioconjugates on  $\beta$ -CD functionalized surfaces. We then prepared Fc-RGD bioconjugates **1-2** that display four copies of guest motifs. In parallel, we designed a control adamantane (Ad) derivative **3** that forms a stronger quasi-irreversible multivalent host-guest complex with  $\beta$ -CD preventing the cell release.

**Synthesis of multi-functional compounds.** To produce the macromolecules **1** and **3**, we used a convergent chemical synthesis *via* sequential chemoselective ligations of the functional units using oxime ligation<sup>14</sup> and copper-catalysed azide-alkyne cycloaddition (Scheme 1).<sup>15</sup> Peptides **5-7** were prepared through a combination of solid and solution-phase syntheses according to methods already developed by our group.<sup>16</sup> One-pot aminoxy deprotection of cyclodecapeptide **6** and subsequent oxime ligation of RGD derivative **5** were carried out in aqueous trifluoroacetic acid (TFA) solution. Full removal of serine protecting groups was completed with concentrated TFA. Subsequent oxidative cleavage with sodium periodate of the amino-alcohol moiety of serine residues provided the compound **8**. The intermediate macromolecule **9** bearing four alkyne functions was then produced through a second oxime ligation between cyclodecapeptides **7** and **8**. Cycloadditions of Fc derivative **10** and Ad derivative **11** with the intermediate **9** provided, respectively, the RGD

compounds **1** and **3** in satisfying yields (see the ESI<sup>†</sup>). In parallel, the compound **2** displaying a single RGD unit and the compound **4** lacking the RGD motif were synthesized as described earlier.<sup>12a</sup>

**Functionalization of surfaces.** SAM functionalized surfaces were then prepared by exposing gold surfaces to a solution containing 20 mol % of  $\beta$ -CD-terminated thiol in combination with oligo(ethylene glycol)-terminated thiol. This percentage represents a fine balance between maximizing the density of  $\beta$ -CD on the SAM surface but avoiding the steric hindrance of the cyclic oligosaccharide aiming to optimize the  $\beta$ -CD host properties on surfaces.<sup>17</sup> Quartz crystal microbalance with dissipation monitoring (QCM-D) was used to monitor the binding of the bifunctional compounds onto the  $\beta$ -CD SAM platform. Figure 2 shows the immobilization of compound **1** on  $\beta$ -CD SAM. The obtained QCM-D signals after rinsing confirm the inclusion complex stability. Additionally, the dissipation shift is very low ( $0.4 \pm 0.1 \times 10^{-6}$ ) indicating that the layer comprising compound **1** is rather rigid. From a combined QCM-D and spectroscopic ellipsometry (SE) measurement, we can convert the QCM-D frequency shift into a molecular surface density (Fig. 3). From a mean frequency shift (measured from 10 independent experiments) of  $-16 \pm 4$  Hz, the molecular surface density of stably bound compound **1** at saturation ( $19 \pm 5$  pmol.cm<sup>-2</sup>) was determined by the calibration plot ( $\Delta f$  vs.  $m_{SE}$ , Fig. 3). A root-mean-square (rms) inter-ligand distance of 3.0 nm can be calculated from this surface density of **1**. By SE, we measured a comparable molecular surface density of  $18.6 \pm 1.0$  pmol.cm<sup>-2</sup> for a compound **4'** of similar structure as compounds **4** and **2** (Fig. S16, ESI<sup>†</sup>), suggesting that the maximal surface density is essentially determined by the size of the decapeptide scaffolds to which Fc and RGD motifs are attached.

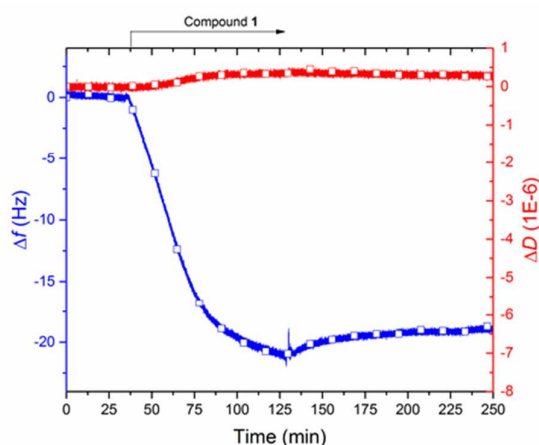


**Fig. 2** QCM-D profile (frequency shift - blue line, dissipation shift - red line) characterizing the build-up of the biosensing layer. The initial  $\beta$ -CD-functionalized SAM was prepared *ex situ* by overnight adsorption of thiols, and adsorption of compound **1** (0.8  $\mu$ M) in PBS buffer solution was then monitored by QCM-D. The arrow indicates start and duration of sample incubation; for remaining times the surface was exposed to pure running buffer.  $T = 24^\circ\text{C}$ , flow rate =  $20 \mu\text{L}\cdot\text{min}^{-1}$ .

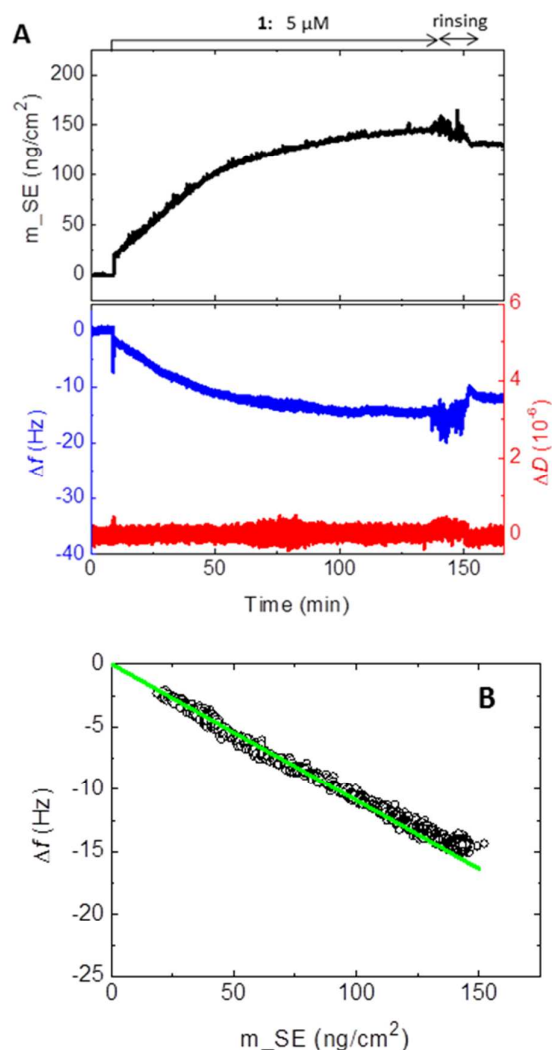


**Fig. 3** Binding of **1** to  $\beta$ -CD SAM monitored simultaneously by QCM-D and SE. (A) Top panel: areal mass density of compound **1**, determined by SE. Bottom panel: QCM-D frequency shift  $\Delta f$  (blue) and dissipation shift  $\Delta D$  (red). Start and duration of injection of compound **1** are indicated by an arrow on top of the graphs. Before sample incubation, and after binding saturation, the surfaces were exposed to pure running buffer; scatter at the start of sample injection and during removal of excess sample ('rinsing') is due to transient perturbations associated with pipetting solutions into the measurement cuvette. (B) Relationship between the QCM-D frequency shift and areal mass density, determined from correlation of the data in A. The relationship is approximately linear is indicated by the straight line (green) through the origin.

**Control of RGD ligand surface densities.** In order to achieve lower RGD ligand surface densities, appropriate ratios of the cell-adhesive compounds **1** or **2** in combination with the non-adhesive compound **4** were used to functionalize the  $\beta$ -CD SAM surfaces.<sup>18</sup> Based on the binding kinetics of each compound, the RGD surface concentrations and the corresponding inter-ligand distances were determined for the different mixtures of compounds **1** or **2** with **4**. The three compounds should interact very similarly with the surface, because they display guest motifs in the same way and have the same footprint. It is therefore reasonable to assume that

adsorption from a mixed solution is a simple overlapping of individual component bindings.

In a first step, we considered the binding processes for each component individually, and performed QCM-D binding assays with pure compounds at selected reference concentrations  $c_{i,ref}$ , where the index  $i$  denotes compound **1**, **2** or **4** (Fig. S17 A-C, ESI<sup>†</sup>). The measurements were performed under flow, at rates identical to those later used for the preparation of surfaces for cell adhesion studies. We found that the frequency response rates  $\left.\frac{df}{dt}\right|_i$  were virtually constant throughout most of the binding process, although distinct, for all three compounds (Fig. S17D-F, ESI<sup>†</sup>; Table 1), that is,

$$\Delta f_i(t) = \left.\frac{df}{dt}\right|_i t, \quad [1]$$

**Table 1** Quantities derived from reference QCM-D measurements.

Compound	$\Delta f_{sat}$ (Hz)	$c_{ref}$	$\left.\frac{df}{dt}\right _{ref}$	$\Omega$
	(Hz)	( $\mu$ M)	(Hz/min)	
<b>1</b>	$-16 \pm 4$	0.8	$-0.46 \pm 0.15$	$0.28 \pm 0.15$
<b>2</b>	$-9.7 \pm 1.0$	3.3	$-3.1 \pm 0.2$	$0.75 \pm 0.18$
<b>4</b>	$-8.1 \pm 1.0$	2.5	$-2.6 \pm 0.2$	-

where  $t$  is the time. Moreover, a combined QCM-D/SE measurement with compound **1** (Fig. 3) demonstrated that the relationship between the areal mass density  $m_{SE}$  and the QCM-D frequency shift  $\Delta f$  is linear to a good approximation. Considering the similarities in structure and surface interaction of **1**, **2** and **4**, we can assume that the close-to-linear relationship also holds for **2** and **4**, that is

$$\Gamma_i = \frac{1}{M_i} \left.\frac{dm_{SE}}{df}\right|_i \Delta f_i, \quad [2]$$

where  $\Gamma$  is the molar surface density and  $M$  the molecular mass. The sensitivity constants  $\left.\frac{dm_{SE}}{df}\right|_i$  can be related to the frequency shifts at saturation  $\Delta f_{i,sat}$  (Table 1, Fig. S17A-C, ESI<sup>†</sup>), through

$$\left.\frac{dm_{SE}}{df}\right|_i = \frac{M_i \Gamma_{i,sat}}{\Delta f_{i,sat}}, \quad [3]$$

by exploiting the fact that  $\Gamma_{sat} = 19 \text{ pmol/cm}^2$  is the same for all compounds. From Eqs. [1] to [3] we obtain

$$\Gamma_i(t) = \frac{1}{M_i} \left.\frac{dm_{SE}}{df}\right|_i \left.\frac{df}{dt}\right|_i t = \frac{\Gamma_{i,sat}}{\Delta f_{i,sat}} \left.\frac{df}{dt}\right|_i t \quad [4]$$

for the adsorption of pure compounds over most of the binding process. We can generalize Eq. [4] and include explicitly the concentration dependence of the binding rate on the solution concentration  $c_i$

$$\Gamma_i(c_i, t) = \frac{\Gamma_{i,sat}}{\Delta f_{i,sat}} \left.\frac{df}{dt}\right|_{i,ref} \frac{c_i}{c_{i,ref}} t \quad [5]$$

where  $c_{i,ref}$  are the reference concentrations at which  $\left.\frac{df}{dt}\right|_{i,ref}$  are measured. Returning to the case of co-adsorption, the superposition of binding processes implies that the total surface density  $\Gamma_{tot}(t) = \Gamma_j(t) + \Gamma_4(t)$  is determined by binding of

compounds **1** and **2** (denoted by index  $j$ ), and **4**, each according to Eq. [5] until saturation is reached. One can show that, at saturation,

$$\Gamma_{j,sat}(c_j) = \Gamma_{tot,sat} \Omega_j \frac{c_j}{c_4} / \left(1 + \Omega_j \frac{c_j}{c_4}\right)$$

with  $\Omega_j \equiv \frac{\Gamma_j c_4}{\Gamma_4 c_j} = \frac{\Delta f_{4,sat}}{\Delta f_{j,sat}} \times \left.\frac{df}{dt}\right|_{j,ref} / \left.\frac{df}{dt}\right|_{4,ref} \times \frac{c_{4,ref}}{c_{j,ref}}$ , [6]

where  $\Omega_j$  can be readily determined from reference QCM-D measurements with pure compounds **1**, **2** and **4**. In essence, the factors  $\Omega_j$  account for the differences in the on rates (including mass transport) of compounds **1** or **2** relative to compound **4**. Table 1 confirms that these are of a similar order of magnitude, as expected, considering that all compounds have roughly the same size and should interact very similarly with the surface.

**Table 2** RGD compound surface densities after co-adsorption, estimated from Eq. [7].

Compound	$c/c_4$	$\Gamma_{sat}/\Gamma_{tot,sat}$	$\Gamma_{sat}$	$r_{rms}$
	(%)	(%)	( $\text{pmol/cm}^2$ )	(nm)
<b>1</b>	-	100	19	3.0
	3.4	0.95	0.18	30
	0.30	0.084	0.016	102
	0.030	0.0084	0.0016	323
	0.0030	0.00084	0.00016	1020
<b>2</b>	-	100	19	3.0
	1.3	1.0	0.19	30
	0.13	0.10	0.019	94
	0.013	0.010	0.0019	299

At high dilutions of the RGD bearing compounds ( $c_j \ll c_4$ ), Eq. [6] can be simplified further to

$$\Gamma_{j,sat}(c_j) \approx \Omega_j \Gamma_{tot,sat} \frac{c_j}{c_4}. \quad [7]$$

Eq. [7] with  $\Gamma_{tot,sat} = 19 \text{ pmol/cm}^2$  and  $\Omega_j$  from Table 1 was used to estimate the surface coverage of **1** or **2** at saturation when co-adsorbed in various mixtures with **4**. Compounds **1** or **2** were thus co-immobilized on  $\beta$ CD-SAM surfaces in the presence of non-adhesive compound **4** using different  $c_j/c_4$  ratio and their adsorption were monitored by QCM-D. The results are shown in Table 2: they include the percentage of RGD compounds **1** or **2** in the solution used to prepare the functionalized surfaces, the molar surface density of each compound and the root-mean-square distance  $r_{rms}$  between adjacent molecules. Taken together, the approach presented here enables quantitative tuning of the RGD ligand surface density over a large range of densities that are difficult to measure directly.

**Effect of RGD presentation on cells.** To evaluate the effect of the multimeric RGD presentation by compound **1** compared to monomeric compound **2**, cell adhesion assays were performed on the different surfaces and monitored using optical microscopy. Experiments were conducted under flow using human embryonic kidney cells HEK-293( $\beta$ 3) that overexpress  $\alpha_v\beta_3$  integrin and HEK-293( $\beta$ 1) were chosen as a negative control ( $\alpha_v\beta_3$ -negative but expressing  $\alpha_v$  and  $\beta_1$  subunits).<sup>19</sup> We first evaluated the cell adhesion (50000

cells/mL) on saturated surfaces presenting compound **1**. The presence of RGD ligands on the surface promotes strong adhesion and spreading morphology of HEK-293( $\beta$ 3) cells in a fluidic system (Fig. 4 A). Under these conditions, the viability of cells was observed after 20 min by using a trypan blue assay (Fig. 4 B). Most cells were alive and only a minor fraction (<20%) were stained signifying cell death.

To avoid cell spreading thus making easier the cell release, we performed the next experiments under drastic conditions by using a shorter injection time (3 min) with lower cell concentration (5000 cells/mL). We first assessed cell adhesion on saturated surfaces displaying either the multimeric compound **1** or the monomeric compound **2** (Fig. S19, ESI<sup>†</sup>). We observed rapid cell adhesion on both surfaces even if we noticed that the cell densities were much lower than in the previous case. This result indicates that the multimeric architecture of compound **1** does not produce an important contribution to ligand–integrin interactions as the multivalency effect essentially comes from the high molecular surface density. This result is in good agreement with previous experiments conducted on resin beads functionalized with RGD compounds.<sup>20</sup> It is worth noting that for surfaces displaying more than 10% of tetrameric RGD compound **1** we obtain saturated surfaces and a strong adhesion that cannot allow cell detachment (data not shown).

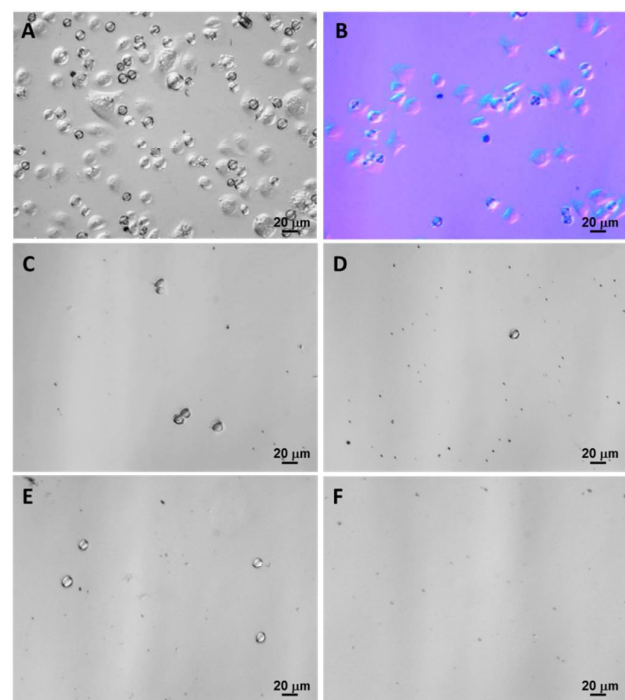


**Fig. 4** Optical microscopy images of HEK-293( $\beta$ 3) cell adhesion to SAM surfaces. (A–B) Cell suspension (50000 cells/mL) was continuously injected for 20 min at a flow rate of  $100 \mu\text{L}\cdot\text{min}^{-1}$  at  $37^\circ\text{C}$  to saturated surfaces presenting compound **1**. (B) Cell viability assay on HEK-293( $\beta$ 3) cells: micrograph was taken during injection of trypan blue. (C–F) Cell suspension (5000 cells/mL) was continuously injected for 3 min at a flow rate of  $100 \mu\text{L}\cdot\text{min}^{-1}$  at  $37^\circ\text{C}$  to SAM surfaces displaying C) 0.95% compound **1**, D) 1% compound **2**, E) 0.0084% compound **1** and F) 0.1% compound **2**. These images were chosen because they are representative of the entire surface.

To discriminate the effect of the tetrameric RGD compound **1** from the multivalency provided by a high molecular surface density, we next assessed cell adhesion using SAMs carrying low densities of RGD compounds (ratios from  $\sim 0.001\%$  to  $1\%$ ). On surfaces displaying  $\sim 1\%$  RGD compounds (inter-compound spacing of  $\sim 30 \text{ nm}$  which corresponds to  $1000 \text{ RGD}/\mu\text{m}^2$ ), we observed clear adhesion of HEK-293( $\beta$ 3) cells to  $\beta$ -CD-SAM surfaces functionalized by the tetrameric RGD compound **1** whereas cell attachment was highly restricted on surfaces functionalized with the monomeric RGD compound **2** (Fig. 4 C–D). As the images are representative of the whole functionalized surface, we could estimate that the cell densities were about five times lower on the surface displaying monomeric compound **2**. Importantly, we did not observe adhesion of HEK-293( $\beta$ 1) confirming that adhesion is mediated by the specific binding of  $\alpha_v\beta_3$  integrin to RGD (Fig. S19–S22, ESI<sup>†</sup>). We next examined  $\beta$ -CD-SAM surfaces functionalized with lower densities of RGD compounds. While we still identified adherent round cells on surfaces displaying  $\sim 0.01\%$  of multimeric RGD compound **1** (Fig. 4 E), we did not observe any cells on surfaces exhibiting  $0.1\%$  of monomeric RGD compound **2** (Fig. 4 F). We calculated a critical root-mean-square (rms) inter-ligand spacing of  $\sim 100 \text{ nm}$  ( $110 \text{ RGD}/\mu\text{m}^2$ ) for compound **2** above which cell binding was effectively impaired. This data is in good agreement with reported results for cell adhesion to surfaces that were functionalized with RGD-containing gold nanoparticles.<sup>10c</sup> Interestingly, an rms inter-ligand spacing of  $\sim 320 \text{ nm}$  ( $10 \text{ RGD}/\mu\text{m}^2$ ) was sufficient for cell attachment to surfaces functionalized with the tetrameric ligand **1**. This result emphasizes the importance of the tetrameric architecture of compound **1**. Therefore, we can effectively discriminate the multivalent effect at a length scale of  $1 \text{ nm}$  (provided by the presentation of RGD as multimeric clusters) from the multivalent effect at larger scales (provided by the surface). To our knowledge, this is the first time that the effect of a multimeric RGD compound on surface was shown in comparison with its monomeric analogue under flow conditions. It is important to note that at this very low RGD density of  $10 \text{ RGD}/\mu\text{m}^2$ , cell spreading was observed 20 min after cell injection (Fig. S23, ESI<sup>†</sup>). Pioneering studies by Hubbell *et al.* have shown that an inter-ligand spacing of  $440 \text{ nm}$  was suitable for fibroblast spreading on glass substrates functionalized with the linear peptide GRGDY, and our results are consistent with this finding.<sup>21</sup>

**Triggered cell release.** For very low RGD density (Fig. 4 E) and short adhesion time duration, cells remain round making their detachment from the surface easier. We then evaluated the ability of the selectively adhesive surface comprising compound **1** for cell release. Application of an oxidizing potential ( $E_{\text{ox}} = + 0.55 \text{ V}$ , see Fig. S24, ESI<sup>†</sup>) results in the oxidation of ferrocene to the ferrocenium cation triggering the detachment of compounds **1** and **4** from the  $\beta$ -CD-SAM (Fig. 5 A) and thus the release of the captured cells (Fig. 5 B–C, see also Fig. S25, ESI<sup>†</sup>). Under the same conditions, we examined a surface displaying the adamantane derivative compound **3** which forms stringer, quasi-irreversible multivalent host-guest

complexes with  $\beta$ -CD. As expected, the oxidative conditions did not allow the cell release (Fig. S26, S27, ESI<sup>†</sup>). These results highlight the potential of the tetrameric RGD compound **1** for the selective isolation of  $\alpha_v\beta_3$ -expressing cells under flow conditions.

## Conclusions

In conclusion, we compared the effect of a multimeric RGD compound to its monomeric analogue on a specific  $\alpha_v\beta_3$ -integrin expressing cell capture and release assay. We have shown that the clustered RGD compound improves specific cell adhesion under short injection time conditions using low cell concentrations, thus allowing cell release. Furthermore by using the clustered RGD compound, an inter-ligand spacing of 320 nm is satisfactory for cell adhesion while 30 nm is required for the monomeric RGD conjugate. We reason that this cell capture/release system could be applied for CTC isolation from blood samples prior to cell characterization and then facilitating clinical decision.<sup>22</sup>

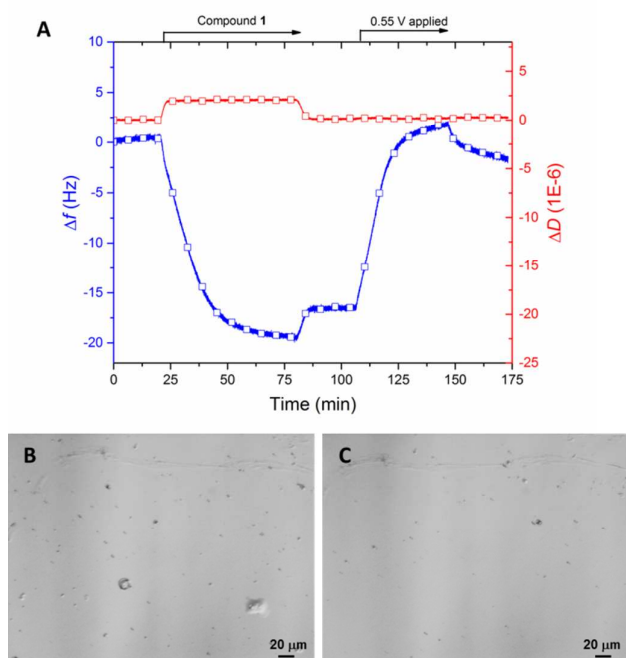


**Fig. 5** (A) Binding of compound **1** (2.5  $\mu$ M) to a  $\beta$ -CD SAM and subsequent electrochemical release. QCM-D (frequency shifts – blue, dissipation shifts – red; overtone  $n = 3$  is shown) is combined with electrochemistry. Compound **1** is largely released upon electrochemical oxidation by applying a potential of 0.55 V vs. AgCl/Ag. The arrows represent the start and duration of sample injection and application of oxidative potential;  $T = 24^\circ\text{C}$ , flow rate =  $20 \mu\text{L}\cdot\text{min}^{-1}$ . (B-C) Electrochemical detachment assay on HEK-293( $\beta_3$ ) cells on 0.0084% compound **1**. Micrographs (B) was taken after cell injection for 3 min. Micrographs (C) was taken on the same spot after applying an oxidative potential (0.55 V vs. AgCl/Ag), gentle rinsing of the surfaces with DMEM outside the measurement chamber and replacing in the QCM-D module for imaging.

## Experimental

### Materials and methods

All Fmoc amino acid derivatives and resins were purchased from Advanced ChemTech Europe (Brussels, Belgium), Bachem Biochimie SARL (Voisins-Les-Bretonneux, France) and France Biochem S.A. (Meudon, France). PyBOP was purchased from France Biochem. HS-(CH<sub>2</sub>)<sub>11</sub>-EG<sub>6</sub>-CH<sub>2</sub>COONHS and HS-(CH<sub>2</sub>)<sub>11</sub>-EG<sub>4</sub>-OH were purchased from Prochimia Surfaces (Prochimia Surfaces, Sopot, Poland). 6-Monodeoxy-6-monoamino- $\beta$ -Cyclodextrin-HCl was provided by Cyclodextrin Shop (Tilburg, The Netherlands). N<sub>3</sub>-EG<sub>4</sub>-NHS was purchased from IRIS Biotech GMBH. PBS (Phosphate Buffer Saline), DMEM (Dulbecco's Modified Eagle's Medium), fetal bovine serum, and Geneticin (G418 sulfate) for cell culture were obtained from Gibco (Illkirch, France). Other reagents were obtained from either Aldrich (Saint Quentin Fallavier, France) or Acros (Noisy-Le-Grand, France).

### General procedure for solid-phase peptide synthesis

Assembly of all protected peptides was carried out using the Fmoc/t-Bu strategy manually in a glass reaction vessel fitted with a sintered glass frit or automatically on a peptide synthesizer using 2-chlorotriylchloride. Coupling reactions were performed manually by using 2 equiv of N-Fmoc-protected amino acid (relative to the resin loading) activated in situ with 2 equiv. of PyBOP and 3-5 equiv. of diisopropylethylamine (DIPEA) in DMF (10 mL/g resin) for 30 min except for the first coupling on 2-chlorotriylchloride. The coupling efficiency in manual synthesis was assessed by TNBS tests. N-Fmoc protecting groups were removed by treatment with a piperidine/DMF solution (1:4) for 10 min (10 mL/g resin). The process was repeated three times and the completeness of deprotection verified by reading the UV absorbance of the piperidine washings at 299 nm. The linear peptides were then released from the resin by treatments with a solution of trifluoroacetic acid/ methylene chloride (1:99, 10 mL/mg resin, 2x30 min). After evaporation, diethyl ether was added to precipitate peptides. Then, they were triturated and washed three times with diethyl ether to obtain crude materials that were used in the next step without further purification.

### General Procedure for Cyclization Reactions

All linear peptides were dissolved in DMF (0.5 mM) and the pH values were adjusted to 8-9 by addition of DIPEA. PyBOP (1.3 equiv.) was added and the solution stirred at room temperature for 1 h. Solvent was removed under reduced pressure and the residue dissolved in a minimum of methylene chloride. Diethyl ether was added to precipitate peptides. They were then triturated and washed three times with diethyl ether to obtain crude materials that was used in the next step without further purification.

### Synthesis of compound **6**

The linear protected decapeptide was assembled as described in the general procedure for solid phase peptide synthesis (600

mg, loading of 0.46 mmol/g) using building blocks as previously described, and was used in the next cyclization step without further purification. The cyclization reaction was carried out as described in the general procedure for peptide cyclization. The cyclic protected peptide **6** was used in the next step without further purification.

#### Synthesis of compound 7

The linear protected decapeptide was assembled as described in the general procedure for solid phase peptide synthesis (600 mg, loading of 0.45 mmol/g) using building blocks as previously described,<sup>12a</sup> and was used in the next cyclization step without further purification. The cyclization reaction was carried out as described in the general procedure for peptide cyclization. The cyclic protected peptide **7** was used in the next step without further purification.

#### Synthesis of compound 8

To a solution of cyclodecapeptide **6** (83 mg, 39  $\mu\text{mol}$ ) in  $\text{H}_2\text{O}$ /trifluoroacetic acid (13 mL; 3:7) was added cyclo[Arg-Gly-Asp-D-Phe-Lys(-CO-CHO)-] peptide derivative **5** (129 mg, 195  $\mu\text{mol}$ ), which was synthesized as previously described.<sup>23</sup> The solution was stirred for 20 min at room temperature. After removal of the solvents under reduced pressure, the removal of the *t*-Bu protecting groups on the RGD-containing conjugate was carried out in 10 mL of a solution containing TFA/ $\text{H}_2\text{O}$  (95:5). The solution was stirred at room temperature for 2 h. The product was directly purified by RP-HPLC as described in the general procedure for purification to yield the RGD-containing conjugate as a white powder (70 mg, 17  $\mu\text{mol}$ , 44%). To a solution of the RGD-containing conjugate (70 mg, 17  $\mu\text{mol}$ ) in water (5.5 mL) was added 20 equiv. of  $\text{NaIO}_4$  (73 mg, 341  $\mu\text{mol}$ ). After 20 min stirring at room temperature, the di-aldehyde product was directly purified by RP-HPLC to yield compound **8** as a white powder (32 mg, 8  $\mu\text{mol}$ , 46%).

#### Synthesis of compound 9

To a solution containing the derivative **8** (25 mg, 7  $\mu\text{mol}$ ) in 14 mL of  $\text{H}_2\text{O}$ / $\text{CH}_3\text{CN}$ /TFA (2:1:7) was added cyclopeptide **7** (11.2 mg, 7  $\mu\text{mol}$ ). The reaction was stirred for 20 min at room temperature. Compound **9** was isolated after purification by RP-HPLC as a white powder (17 mg, 3  $\mu\text{mol}$ , 42%).

#### Synthesis of compound 1

To a solution of alkyne-containing compound **9** (2 mg, 0.36  $\mu\text{mol}$ ) and adamantyl azide fragments Fc- $\text{EG}_4\text{-N}_3$  **10** (1 mg, 2.2  $\mu\text{mol}$ ) prepared as previously described<sup>24</sup> in degassed DMF under nitrogen atmosphere, was added a solution of  $\text{CuSO}_4$  (1 equiv.) and THPTA (3 equiv.) in degassed phosphate buffer (100 mM, pH 7.4). A solution of sodium ascorbate (10 equiv.) in degassed phosphate buffer was added to the medium. The resulting mixture was heated at 45°C for 2h30. After completion, the crude was directly subjected to preparative RP-HPLC with a step gradient of ACN in water containing 0.1% TFA to afford pure peptide derivatives **1** as a white powder (1.7 mg, 0.23  $\mu\text{mol}$ , 63% yield).

#### Synthesis of compound 2

The compound **2** was prepared as previously described.<sup>12a</sup>

#### Synthesis of compound 3

To a solution of alkyne-containing compound **9** (2.5 mg, 0.45  $\mu\text{mol}$ ) and AD- $\text{EG}_4\text{-N}_3$  **11** (1.2 mg, 2.7  $\mu\text{mol}$ ) prepared as previously described<sup>17b</sup> in degassed DMF under nitrogen atmosphere, was added a solution of  $\text{CuSO}_4$  (1 equiv.) and THPTA (3 equiv.) in degassed phosphate buffer (100 mM, pH 7.4). A solution of sodium ascorbate (10 equiv.) in degassed phosphate buffer was added to the medium. The resulting mixture was heated at 45°C for 2h30. After completion, the crude was directly subjected to preparative RP-HPLC with a step gradient of ACN in water containing 0.1% TFA to afford pure peptide derivatives **3** as a white powder (2.3 mg, 0.32  $\mu\text{mol}$ , 71% yield).

#### Synthesis of compound 4

Compound **4** was obtained from the requisite linear protected decapeptide assembled as described in the general procedure for solid phase peptide synthesis (380 mg, loading of 0.45 mmol/g) using building blocks as previously described.<sup>16</sup> The linear protected decapeptide was used in the next cyclization step without further purification. The cyclization reaction was carried out as described in the general procedure for peptide cyclization. The cyclic protected peptide was used in the next step without further purification. The removal of the *t*-Bu protecting groups on the serine residues of the cyclic decapeptide was carried out in 4 mL of a solution containing TFA/ $\text{H}_2\text{O}$ /TIS (95:2.5:2.5). The solution was stirred at room temperature for 2 h. After removal of the solvents under reduced pressure; the product was isolated by precipitation from diethyl ether. The crude was subjected to RP-HPLC purification to afford the deprotected peptide as a white powder. Deprotected peptide (4.5 mg, 3.4  $\mu\text{mol}$ ) and azido derivative **10** (9 mg, 17  $\mu\text{mol}$ ), were condensed as described in the procedure for CuAAC ligation of **1** or **3** to yield after purification compound **4** as a white powder (7 mg, 2.2  $\mu\text{mol}$ , 65% yield).

#### Synthesis of $\beta$ -CD terminated alkanethiol

The  $\beta$ -CD terminated alkanethiol was prepared as previously described.<sup>17b</sup>

#### Quartz crystal microbalance with dissipation monitoring (QCM-D)

QCM-D measurements were performed using Q-Sense E1 or E4 instruments (Biolin Scientific Västra Frölunda, Sweden) equipped with one or four flow modules, respectively. Besides measurement of bound mass (including trapped solvent), which is provided from changes in the resonance frequency,  $f$ , of the sensor crystal, the QCM-D technique also provides structural information of biomolecular films via changes in the energy dissipation,  $D$ , of the sensor crystal.  $f$  and  $D$  were measured at the fundamental resonance frequency (4.95 MHz) as well as at the third, fifth, seventh, ninth, eleventh, and thirteenth overtones ( $n = 3, 5, 7, 9, 11$  and 13). Normalized frequency shifts  $\Delta f = \Delta f_n/n$  and dissipation

shifts  $\Delta D = \Delta D_n$  of the seventh overtone are presented unless otherwise stated.

Experiments were conducted in a continuous flow of buffer with a flow rate of  $20 \mu\text{L}\cdot\text{min}^{-1}$  by using a peristaltic pump (ISM935C, Ismatec, Switzerland). The temperature of the E1-E4 QCM-D platform and all solutions were stabilized to ensure stable operation at  $24^\circ\text{C}$ .

For cell-adhesion assays, the sensors were equilibrated in the QCM-D measurement chamber with DMEM medium (without serum) at  $37^\circ\text{C}$ .  $f$  and  $D$  were recorded continuously during the incubation (using a flow rate of  $100 \mu\text{L}/\text{min}$ ) of the cells (5000 or 50000 cells/mL) suspended in the same medium.

Microscopy experiments coupled with QCM-D were performed using the Q-Sense Window Module 401 (Biolin Scientific) and a microscope Axio Imager A1m (Carl Zeiss S.A.S., France). The images were registered and treated using the software Axiovision from Carl Zeiss S.A.S.

Combination of electrochemical and QCM-D measurements (E-QCM-D) were performed using electrochemical QCM-D modules (Biolin Scientific), connected with a CHI 440 potentiostat (CH-Instruments, Inc., USA). Electrode potentials were referred to Ag/AgCl/KCl (3 M). The counter electrode was platinum and the working electrode was the functionalized gold-coated QCM-D sensor. All buffers were previously degassed in order to avoid bubble formation in the fluidic system. All QCM-D experiments were repeated at least three times, and errors indicated in the main text and tables represent standard deviations.

### Spectroscopic Ellipsometry (SE)

SE measures changes in the polarization of light upon reflection at a planar surface, and was employed in aqueous environment with a M2000V system (J.A. Woollam, Lincoln, NE) to quantify the surface density of peptide conjugates in a time-resolved manner. SE measurements were either performed independently, or combined with QCM-D on the same substrate, at room temperature. The functionalization of the gold-coated substrates with  $\beta$ -CD SAM was performed *ex situ*, before the measurement, and the functionalization with the peptide conjugates was then monitored *in situ*. For independent SE measurements, a custom-built open cuvette ( $\sim 120 \mu\text{L}$ ) featuring a magnetic stirrer for homogenization of the cuvette content and a flow-through system for rapid solution exchange during rinsing steps was used.<sup>25</sup> Combined SE/QCM-D measurements were performed with a custom-built open cuvette ( $\sim 2 \text{ mL}$ ), as described in detail elsewhere.<sup>26,27</sup> A magnetic stirrer was used to homogenize the cuvette content for a few seconds during sample injection and also during rinsing steps, whereas adsorption proceeded in still solution to guarantee a homogeneously accessible surface and thus enable quantitative correlation of SE and QCM-D responses which were measured on overlapping but non-identical surface areas.<sup>26</sup>

Peptide conjugate surface densities were quantified through fitting of the SE data to an optical model using the software CompleteEASE (Woollam) as described in detail elsewhere.<sup>28</sup> The model relates the

ellipsometric angles  $\Delta$  and  $\psi$ , measured over the wavelength range  $\lambda = 380$  to  $1000 \text{ nm}$ , to the optical properties of the sensor surface, the adsorbed film, and the surrounding solution. The opaque metal film and the  $\beta$ -CD SAM on gold-coated silicon wafers were treated as a single isotropic layer and fitted as a B-spline substrate; the peptide conjugate film was treated as separate, transparent Cauchy layer. Areal mass densities were determined through de Feijter's equation,<sup>27</sup> using a refractive index increment  $dn/dc = 0.18 \text{ cm}^3/\text{g}$ . All measurements were repeated twice and the data represent mean  $\pm$  standard errors.

### Surface functionalization

QCM-D sensors with  $100 \text{ nm}$  gold-coating (QXS301) were purchased from Biolin Scientific. Appropriately sized silicon wafers with an optically opaque gold coating ( $100 \text{ nm}$ , sputter-coated) were used for SE measurements. Prior to use, the surfaces were exposed to a UV-ozone treatment for  $10 \text{ min}$  using a UV-ozone cleaner (Jelight Company, Irvine, CA, USA). The surfaces were then immersed overnight in a  $1 \text{ mM}$  ethanolic solution of thiols ( $\text{HS}-(\text{CH}_2)_{11}-\text{EG}_4-\text{OH}:\text{HS}-(\text{CH}_2)_{11}-\text{EG}_6-\text{CONH}-\text{CD}$ , 8:2), and then carefully rinsed with ethanol and dried under nitrogen.

### Cell lines and culture conditions

HEK-293( $\beta 3$ ) is a subclone of the human embryonic kidney HEK-293 cell line, stably transfected by a plasmid encoding for the human integrin  $\alpha_v\beta_3$  (kindly provided by the Institut Albert Bonniot, Centre de Recherche INSERM-UJF U823, UJF Site Santé, BP 170, La Tronche, Grenoble 38042 Cedex 9, France). HEK-293 stably transfected by a plasmid encoding the human integrin  $\alpha_v\beta_1$  (HEK-293( $\beta 1$ )) were used as negative control. Both cell lines were cultured as adherent monolayers in DMEM supplemented with  $10\%$  fetal bovine serum (FBS) and  $700 \mu\text{g}/\text{mL}$  Geneticin (G418 sulfate), at  $37^\circ\text{C}$  in a humidified  $95\%$  air/ $5\%$   $\text{CO}_2$  atmosphere. The cell adhesion assays were conducted at a concentration of  $5000$  or  $50000$  cells/mL in DMEM without serum to ensure the specific interaction of integrin-presenting cells with the RGD-presenting surface. As the serum contains adhesion proteins, we must avoid the non-specific adsorption of these proteins onto the functionalized surface.

### Cell viability assay

The viability of the captured cells was assessed in a trypan blue assay. After  $20 \text{ min}$  flow of HEK-293( $\beta 3$ ) cells ( $50000$  cells/mL in DMEM without serum) at  $37^\circ\text{C}$  (flow rate  $100 \mu\text{L}/\text{min}$ ) on a  $\beta$ -CD SAM surface saturated in compound **1**, leading to cell adhesion to the RGD-saturated surface, a trypan blue solution (trypan blue solution  $0.4\%$  in DMEM  $1/1$ ) was injected (flow rate  $100 \mu\text{L}/\text{min}$ ). As viable cells do not take up dyes whereas non-viable cells do, non-viable cells were blue while viable cells were unstained. Pictures were taken after  $3 \text{ min}$  incubation in trypan blue.

## Acknowledgements

This work was supported by research funding from the Agence Nationale de la Recherche, "Blanc SIMI 7" (ANR-13-BS07-0014), "Blanc SVSE 5" (ANR-12-BSVE5-0021), "Arcane" LabEx (ANR-11-LABX-0003-01) and Nanosciences Foundation (Grenoble) for a PhD scholarship to D.T. The authors wish to acknowledge the support from the ICMG Chemistry Nanobio Platform, Grenoble, on which the peptide synthesis has been performed. RPR acknowledges funding by the Spanish Ministry for Economy and Competitiveness for (project MAT2014-54867-R).

## Notes and references

- 1 M. Mammen, S. K. Choi and G. M. Whitesides, *Angew. Chem. Int. Ed.*, 1998, **37**, 2754.
- 2 a) J. S. Desgrosellier and D. A. Cheresh, *Nat. Rev. Cancer*, 2010, **10**, 9; b) J. S. Desgrosellier, L. A. Barnes, D. J. Shields, M. Huang, S. K. Lau, N. Prévost, D. Tarin, S. J. Shattil and D. A. Cheresh, *Nat. Med.*, 2009, **15**, 1163.
- 3 J. Pilch, R. Habermann and B. Felding-Habermann, *J. Biol. Chem.*, 2002, **24**, 21930.
- 4 a) K. Temming, R. M. Schiffelers, G. Molema and R. J. Kok, *Drug Resist. Updates*, 2005, **8**, 381; b) F. Danhier, A. Le Breton and V. Préat, *Mol. Pharmaceutics*, 2012, **9**, 2961.
- 5 M. Pfaff, K. Tangemann, B. Müller, M. Gurrath, G. Müller, H. Kessler, R. Timpl and J. Engel, *J. Biol. Chem.*, 1994, **269**, 20233.
- 6 S. Liu, *Mol. Pharmaceutics*, 2006, **3**, 472.
- 7 a) H. D. Maynard, S. Y. Okada and R. H. Grubbs, *J. Am. Chem. Soc.*, 2001, **123**, 1275; b) R. J. Kok, A. J. Schraa, E. J. Bos, H. E. Moorlag, S. A. Åsgeirsdóttir, M. Everts, D. K. F. Meijer and G. Molema, *Bioconjugate Chem.*, 2002, **13**, 128; c) G. Thumshirn, U. Hersel, S. L. Goodman and H. Kessler, *Chem. Eur. J.*, 2003, **9**, 2717; d) D. Boturyn, J.-L. Coll, E. Garanger, M.-C. Favrot and P. Dumy, *J. Am. Chem. Soc.*, 2004, **126**, 5730; e) Y. Wu, X. Z. Zhang, Z. M. Xiong, Z. Cheng, D. R. Fisher, S. Liu, S. S. Gambhir and X.-Y. Chen, *J. Nucl. Med.*, 2005, **46**, 1707; f) Y. Ye, S. Bloch, B. Xu, S. Achilefu, *J. Med. Chem.*, 2006, **49**, 2268; g) I. Dijkgraaf, A. Y. Rijnders, A. Soede, A. C. Dechesne, G. Wilma van Esse, A. J. Brouwer, F. H. M. Corstens, O. C. Boerman, D. T. S. Rijkers and R. M. J. Liskamp, *Org. Biomol. Chem.*, 2007, **5**, 935; i) S. Chakraborty, J. Shi, Y.-S. Kim, Y. Zhou, B. Jia, F. Wang and S. Liu, *Bioconjugate Chem.*, 2010, **21**, 969; j) D. J. Welsh and D. K. Smith, *Org. Biomol. Chem.*, 2011, **9**, 4795.
- 8 C. H. F. Wenk, F. Ponce, S. Guillermet, C. Tenaud, D. Boturyn, P. Dumy, D. Watrelot-Virieux, C. Carozzo, V. Josserand and J.-L. Coll, *Cancer Lett.*, 2013, **334**, 188.
- 9 a) S. Foillard, Z. Jin, E. Garanger, D. Boturyn, M. Favrot, J.-L. Coll and P. Dumy, *ChemBioChem*, 2008, **9**, 2326; b) S. Dufort, L. Sancey, A. Hurbin, S. Foillard, D. Boturyn, P. Dumy and J.-L. Coll, *J. Drug Target.*, 2011, **19**, 582.
- 10 a) G. Maheshwari, G. Brown, D. A. Lauffenburger, A. Wells and L. G. Griffith, *J. Cell Sci.*, 2000, **113**, 1677; b) E. A. Cavalcanti-Adam, A. Micoulet, J. Blümmel, J. Auernheimer, H. Kessler and J. P. Spatz, *Eur. J. Cell Biol.*, 2006, **85**, 219; c) J. Huang, S. V. Gräter, F. Corbellini, S. Rinck, E. Bock, R. Kemkemer, H. Kessler, J. Ding and J. P. Spatz, *Nano Lett.*, 2009, **9**, 1111; d) J. A. Deeg, I. Louban, D. Aydin, C. Selhuber-Unkel, H. Kessler and J. P. Spatz, *Nano Lett.*, 2011, **11**, 1469; e) M. Schwartzman, M. Palma, J. Sable, J. Abramson, X. Hu, M. P. Sheetz and S. J. Wind, *Nano Lett.*, 2011, **11**, 1306.
- 11 a) Q. An, J. Brinkmann, J. Huskens, S. Krabbenborg, J. de Boer, and P. Jonkheijm, *Angew. Chem. Int. Ed.*, 2012, **51**, 12233; b) J. Boekhoven, C. M. Rubert Perez, S. Sur, A. Worthy and S. I. Stupp, *Angew. Chem. Int. Ed.*, 2013, **52**, 12077-12080; c) P. Neiryneck, J. Brinkmann, Q. Au, D. W. J. Van der Schaft, L.-G. Milroy, P. Jonkheijm and L. Brunsveld, *Chem. Commun.*, 2013, **49**, 3679-3681; d) H. Li, J. Frith and J. J. Cooper-White, *Biomacromolecules*, 2013, **15**, 43-52; e) H. Dong, Y. Li, J. Yu, Y. Song, X. Cai, J. Liu, J. Zhang, R.C. Ewing and D. Shi, *Small*, 2013, **9**, 446-456; f) P. Neiryneck, J. Schimer, P. Jonkheijm, L.-G. Milroy, P. Cigler and L. Brunsveld, *J. Mater. Chem. B*, 2015, **3**, 539.
- 12 a) D. Thakar, L. Coche-Guerente, M. Claron, C. H. F. Wenk, J. Dejeu, P. Dumy, P. Labbé and D. Boturyn, *ChemBioChem*, 2014, **15**, 377; b) J. Brinkmann, E. Cavatorta, S. Sankaran, B. Schmidt, J. van Weerd and P. Jonkheijm, *Chem. Soc. Rev.*, 2014, **43**, 4449-4469; c) T. Gao, L. Li, B. Wang, J. Zhi, Y. Xiang and G. Li, *Anal. Chem.*, 2016, **88**, 9996.
- 13 a) D. Osella, A. Carretta, C. Nervi, M. Ravera and R. Gobetto, *Organometallics*, 2000, **19**, 2791; b) M. J. W. Ludden, D. N. Reinhoudt and J. Huskens, *Chem. Soc. Rev.*, 2006, **35**, 1122-1134.
- 14 K. Rose, *J. Am. Chem. Soc.*, 1994, **116**, 30.
- 15 a) C. W. Tørnøe, C. Christensen and M. Meldal, *J. Org. Chem.*, 2002, **67**, 3057; b) V. V. Rostovtsev, L. G. Green, V. V. Fokin and K. B. Sharpless, *Angew. Chem. Int. Ed.*, 2002, **41**, 2596.
- 16 a) S. Foillard, M. Olsten Rasmussen, J. Razkin, D. Boturyn and P. Dumy, *J. Org. Chem.*, 2008, **73**, 983; b) M. Galibert, P. Dumy and D. Boturyn, *Angew. Chem. Int. Ed.*, 2009, **48**, 2576.
- 17 a) M. R. de Jong, J. Huskens and D. N. Reinhoudt, *Chem. Eur. J.*, 2001, **7**, 4164; b) J. Bacharouche, M. Degardin, L. Jierry, C. Carteret, P. Lavalie, J. Hemmerle, B. Senger, R. Auzely-Velty, F. Boulmedais, D. Boturyn, L. Coche-Guerente, P. Schaaf and G. Francius, *J. Mater. Chem. B*, 2015, **3**, 1801.
- 18 We have shown that SAM comprising the peptide **4** do not allow cell adhesion (Fig. S21, ESI<sup>†</sup>).
- 19 E. Garanger, D. Boturyn, Z.-H. Jin, P. Dumy, M.-C. Favrot and J.-L. Coll, *Mol. Ther.*, 2005, **12**, 1168.
- 20 S. Foillard, P. Dumy and D. Boturyn, *Org. Biomol. Chem.*, 2009, **7**, 4159.
- 21 S. P. Massia and J. A. Hubbell, *J. Cell Biol.*, 1991, **114**, 1089.
- 22 B. Hong and Y. Zu, *Theranostics*, 2013, **3**, 377.
- 23 D. Boturyn and P. Dumy, *Tet. Lett.*, 2011, **42**, 2787.
- 24 G. V. Dubacheva, M. Galibert, L. Coche-Guerente, P. Dumy, D. Boturyn and P. Labbe, *Chem. Commun.*, 2011, **47**, 3565.
- 25 E. Migliorini, D. Thakar, R. Sadir, T. Pleiner, F. Baleux, H. Lortat-Jacob, L. Coche-Guerente and R. P. Richter, *Biomaterials*, 2014, **35**, 8903.
- 26 I. Carton, A. R. Brisson and R. P. Richter, *Anal. Chem.*, 2010, **82**, 9275.
- 27 R. Richter, K. Rodenhausen, N. B. Eisele and M. Schubert, In: K. Hinrichs, K.-J. Eichhorn, editors. *Ellipsometry of functional organic surfaces and films*, Berlin: Springer, 2014, pp. 223.
- 28 G. V. Dubacheva, T. Curk, B. M. Mognetti, R. Auzely-Velty, D. Frenkel and R. P. Richter, *J. Am. Chem. Soc.*, 2014, **136**, 1722.

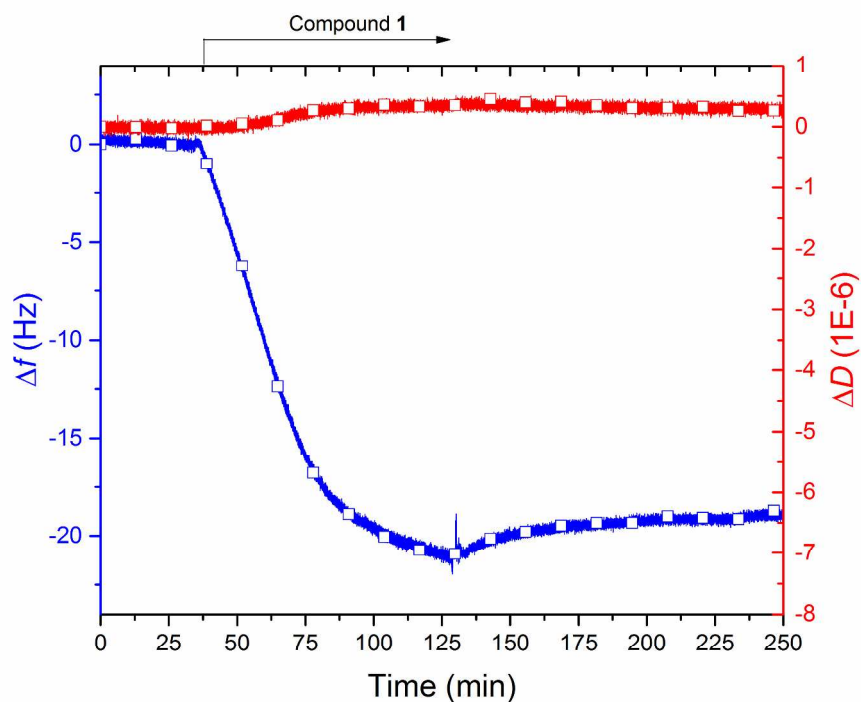


Fig. 2 QCM-D profile (frequency shift - blue line, dissipation shift - red line) characterizing the build-up of the biosensing layer. The initial  $\beta$ -CD-functionalized SAM was prepared ex situ by overnight adsorption of thiols, and adsorption of compound **1** ( $0.8 \mu\text{M}$ ) in PBS buffer solution was then monitored by QCM-D. The arrow indicates start and duration of sample incubation; for remaining times the surface was exposed to pure running buffer.  $T = 24^\circ\text{C}$ , flow rate =  $20 \mu\text{L}\cdot\text{min}^{-1}$ .

272x208mm (300 x 300 DPI)

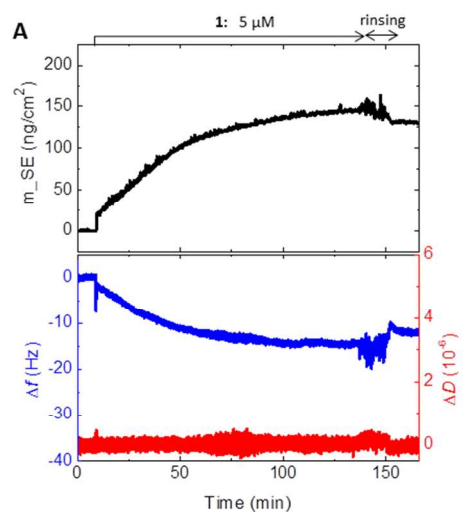
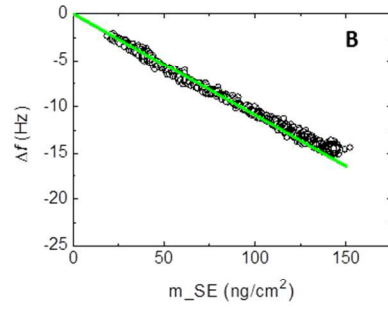


Fig. 3 Binding of **1** to  $\beta$ -CD SAM monitored simultaneously by QCM-D and SE. (A) Top panel: areal mass density of compound **1**, determined by SE. Bottom panel: QCM-D frequency shift  $\Delta f$  (blue) and dissipation shift  $\Delta D$  (red). Start and duration of injection of compound **1** are indicated by an arrow on top of the graphs. Before sample incubation, and after binding saturation, the surfaces were exposed to pure running buffer; scatter at the start of sample injection and during removal of excess sample ('rinsing') is due to transient perturbations associated with pipetting solutions into the measurement cuvette.

254x190mm (96 x 96 DPI)



(B) Relationship between the QCM-D frequency shift and areal mass density, determined from correlation of the data in A. The relationship is approximately linear is indicated by the straight line (green) through the origin.

254x190mm (96 x 96 DPI)

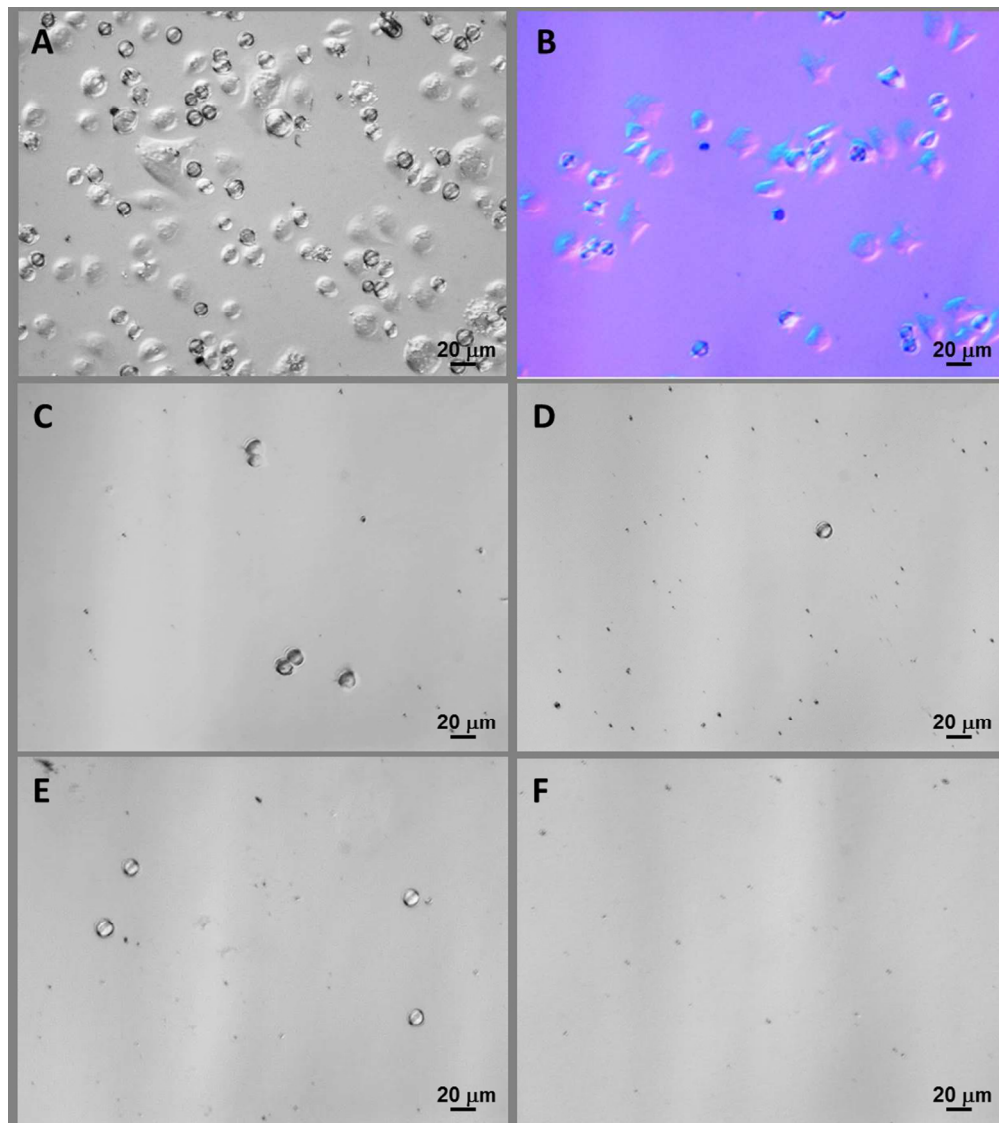


Fig. 4 Optical microscopy images of HEK-293( $\beta$ 3) cell adhesion to SAM surfaces. (A-B) Cell suspension (50000 cells/mL) was continuously injected for 20 min at a flow rate of  $100 \mu\text{L}\cdot\text{min}^{-1}$  at  $37^\circ\text{C}$  to saturated surfaces presenting compound **1**. (B) Cell viability assay on HEK-293( $\beta$ 3) cells: micrograph was taken during injection of trypan blue. (C-F) Cell suspension (5000 cells/mL) was continuously injected for 3 min at a flow rate of  $100 \mu\text{L}\cdot\text{min}^{-1}$  at  $37^\circ\text{C}$  to SAM surfaces displaying C) 0.95% compound **1**, D) 1% compound **2**, E) 0.0084% compound **1** and F) 0.1% compound **2**. These images were chosen because they are representative of the entire surface.

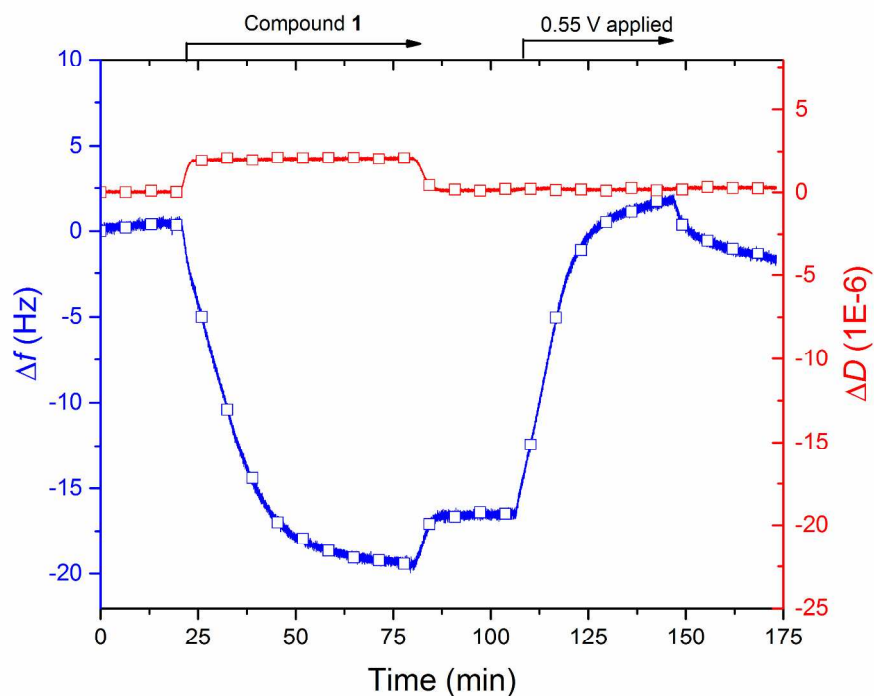
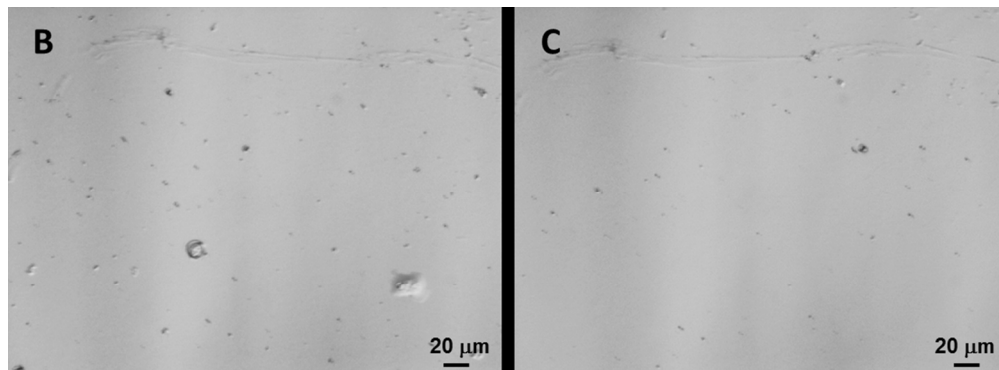


Fig. 5 (A) Binding of compound **1** ( $2.5 \mu\text{M}$ ) to a  $\beta$ -CD SAM and subsequent electrochemical release. QCM-D (frequency shifts – blue, dissipation shifts – red; overtone  $n = 3$  is shown) is combined with electrochemistry. Compound **1** is largely released upon electrochemical oxidation by applying a potential of  $0.55 \text{ V}$  vs.  $\text{AgCl/Ag}$ . The arrows represent the start and duration of sample injection and application of oxidative potential;  $T = 24^\circ\text{C}$ , flow rate =  $20 \mu\text{L}\cdot\text{min}^{-1}$ .

272x208mm (300 x 300 DPI)



(B-C) Electrochemical detachment assay on HEK-293( $\beta$ 3) cells on 0.0084% compound **1**. Micrographs (B) was taken after cell injection for 3 min. Micrographs (C) was taken on the same spot after applying an oxidative potential (0.55 V vs. AgCl/Ag), gentle rinsing of the surfaces with DMEM outside the measurement chamber and replacing in the QCM-D module for imaging.

186x68mm (150 x 150 DPI)

## Supplementary Information

### **Development of a selective cell capture and release assay: impact of clustered RGD ligand**

M. Degardin,<sup>a</sup> D. Thakar,<sup>a</sup> M. Claron,<sup>a</sup> R. P. Richter,<sup>b,c,d</sup> L. Coche-Guérente<sup>a\*</sup> and D. Boturyn<sup>a\*</sup>

[a] Univ. Grenoble-Alpes, CNRS, DCM UMR 5250, F-38000 Grenoble, France.

E-mail: didier.boturyn@univ-grenoble-alpes.fr

[b] University of Leeds, School of Biomedical Sciences and School of Physics and Astronomy, Leeds, United Kingdom.

[c] CIC biomaGUNE, Biosurfaces Lab, San Sebastian, Spain.

[d] Univ. Grenoble-Alpes, CNRS, LIPhy UMR 5588, F-38000 Grenoble, France.

# Table of Contents

<b>Table of Contents</b>	<b>S2</b>
<b>1. Materials and methods for HPLC, QCM-D and SE</b>	<b>S3</b>
1.1 HPLC methods	S3
<b>2. HPLC profiles and MS analysis</b>	<b>S4</b>
2.1 Cyclopeptide <b>6</b>	S4
2.2 Cyclopeptide <b>8</b>	S5
2.3 Cyclopeptide <b>7</b>	S6
2.4 Conjugate <b>9</b>	S7
2.5 Conjugate <b>1</b>	S8
2.6 Conjugate <b>3</b>	S10
2.7 Conjugate <b>4</b>	S12
<b>3. Supplementary QCM-D data and quantification of adsorbed compound 1, 2 and 4</b>	<b>S13</b>
3.1 Absence of non-specific adsorption of compound <b>1</b> on oligoethylene glycol functionalized SAM surface	S13
3.2 Quantification of RGD surface densities	S14
<b>4. Optical micrographs of cell adhesion on surfaces displaying compound 1 or 2.</b>	<b>S15</b>
<b>5. Electrochemical release of RGD compounds</b>	<b>S17</b>
<b>Supplementary reference</b>	<b>S19</b>

# 1. Materials and methods for HPLC, QCM-D and SE

## 1.1 HPLC methods

RP-HPLC analyses were performed on Waters equipment consisting of a Waters 600 controller, a Waters 2487 Dual Absorbance Detector and a Waters In-Line Degasser (Saint-Quentin-en-Yvelines, France). The analytical column used was a Nucleosil 120 Å 3 µm C18 particles, 125 × 4 mm operated at 1 mL/min with linear gradient programs in 20 min run time (routine program: 5% to 100 % B in 20 min). UV monitoring was performed most of the time at 214 nm and 250 nm simultaneously. Solvent A consisted of H<sub>2</sub>O containing 0.1% TFA and solvent B consisted of CH<sub>3</sub>CN containing 9.9% H<sub>2</sub>O and 0.1% TFA. Water was of Milli-Q quality. CH<sub>3</sub>CN and TFA were of HPLC use quality.

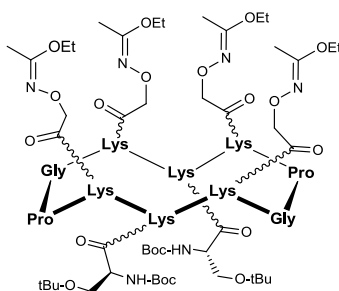
RP-UHPLC analyses were performed on Waters equipment consisting of a Waters Acquity H-Class Bio UPLC combined to a Waters SQ Detector 2 mass spectrometer. The analytical column used was a ACQUITY UPLC BEH C18 Column, 130 Å, 1.7 µm, 2.1 mm x 50 mm operated at 0.6 mL/min with linear gradient programs in 2.20 min run time (routine program: 5% to 100 % B in 2.20 min). UV monitoring was performed at 214 nm. Solvent A consisted of H<sub>2</sub>O containing 0.1% formic acid (FA) and solvent B consisted of CH<sub>3</sub>CN containing 0.1% FA. Water was of Milli-Q quality. CH<sub>3</sub>CN and FA were LC-MS grade.

RP-HPLC purifications were either performed on Gilson GX-281 (high quantities: hundreds of mg) or GX-271 equipment (low quantities: few mg). For GX-281, the preparative column, Macherey-Nagel 100 Å 7 µm C18 particles, 250 × 21 mm was operated at 20.84 mL/min. For GX-271, the preparative column, Macherey-Nagel 300 Å 7 µm C18 particles, 250 × 10 mm (Hoerdt, France) was operated at 4.65 mL/min. Linear gradient programs in 30 min run time were used and solvents A and B were the same as the ones used in RP-HPLC analysis.

Electron spray ionization (ESI-MS) mass spectra were recorded on an Esquire 3000 (Bruker) spectrometer (Champs-sur-Marne, France). The multiply charged data produced by the mass spectrometer on the m/z scale were converted to the molecular weight.

## 2. HPLC profiles and MS analysis

### 2.1 Cyclopeptide 6



#### RP-HPLC profile and ESI-MS analysis of crude 6

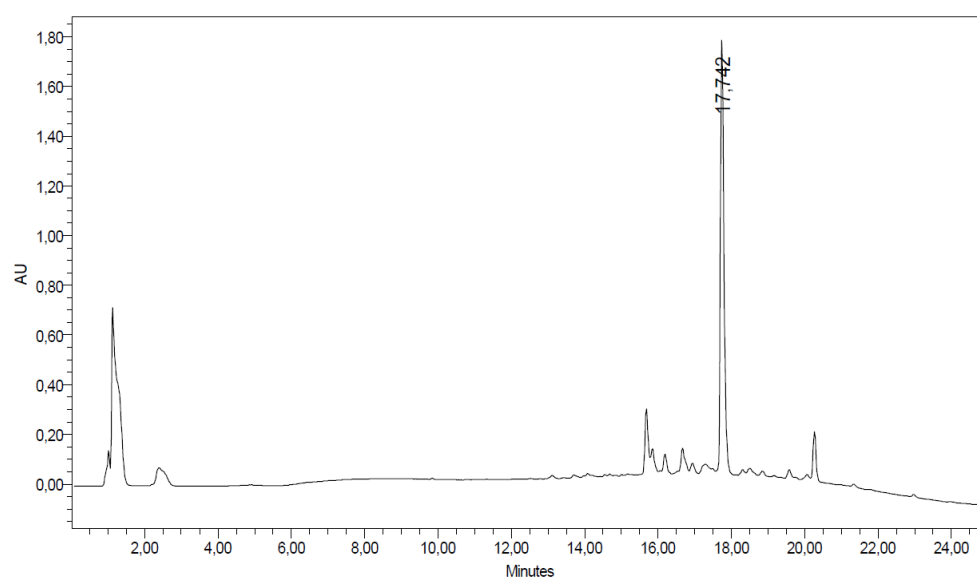


Figure S1: RP-HPLC profile of crude 6.

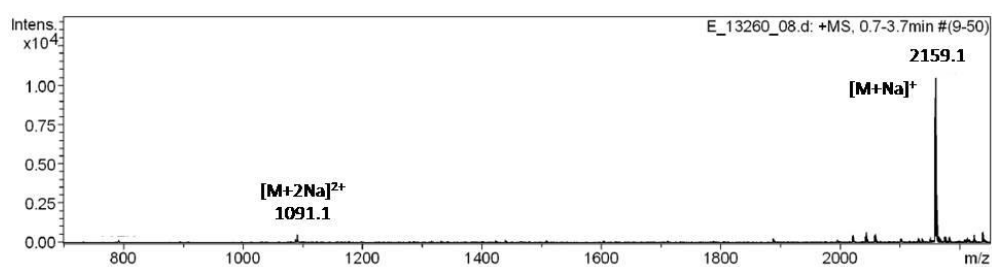
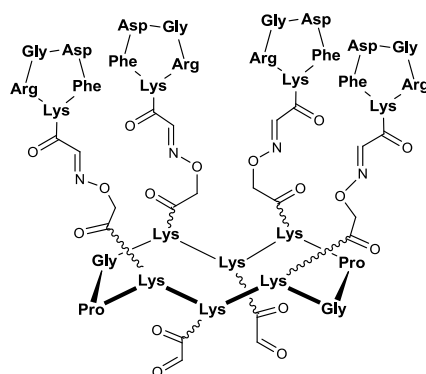


Figure S2: ESI-MS analysis of crude 6.

Mass spectrum (ESI, positive mode) calculated mass for C<sub>98</sub>H<sub>170</sub>N<sub>22</sub>O<sub>30</sub>: 2136.3; found: 2136.1.

## 2.2 Cyclopeptide 8



RP-HPLC profile and ESI-MS analysis of 8

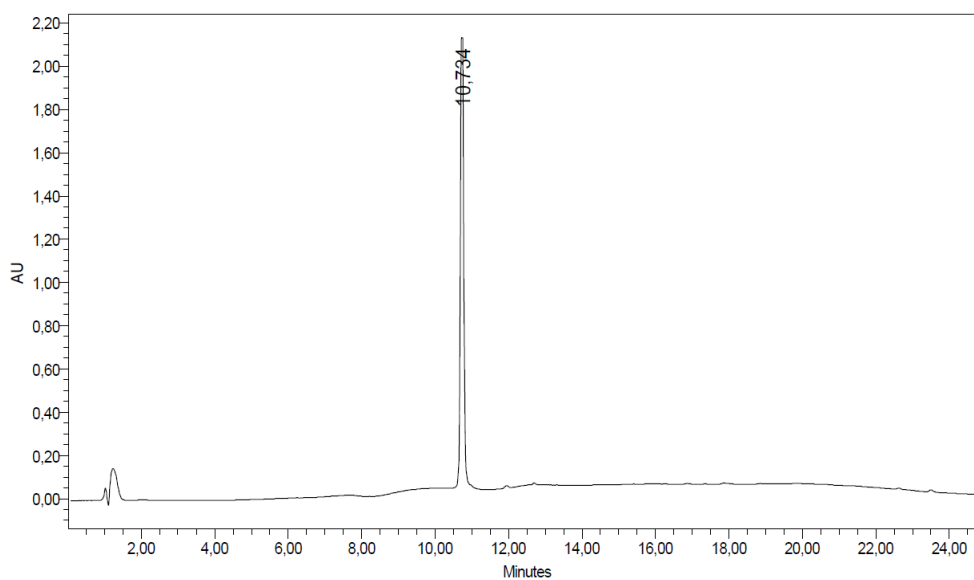


Figure S3: RP-HPLC profile of 8.

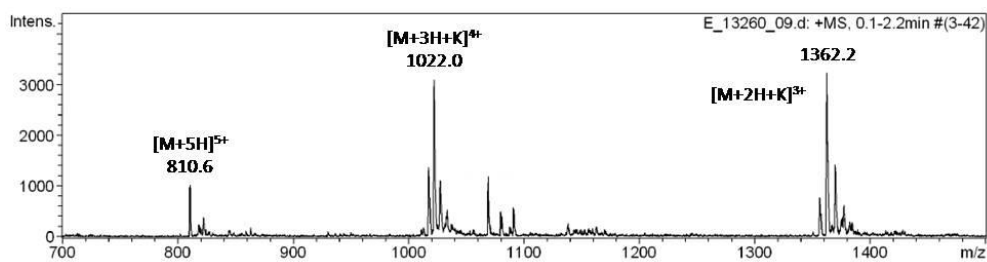
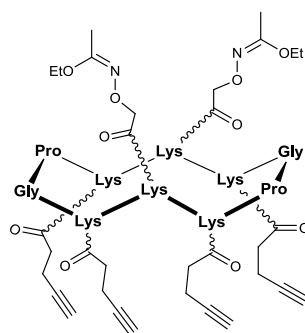


Figure S4: ESI-MS analysis of 8.

Mass spectrum (ESI, positive mode) calculated mass for  $C_{178}H_{260}N_{56}O_{54}$ : 4048.3; found: 4049.2.

## 2.3 Cyclopeptide 7



RP-HPLC profile and ESI-MS analysis of crude 7

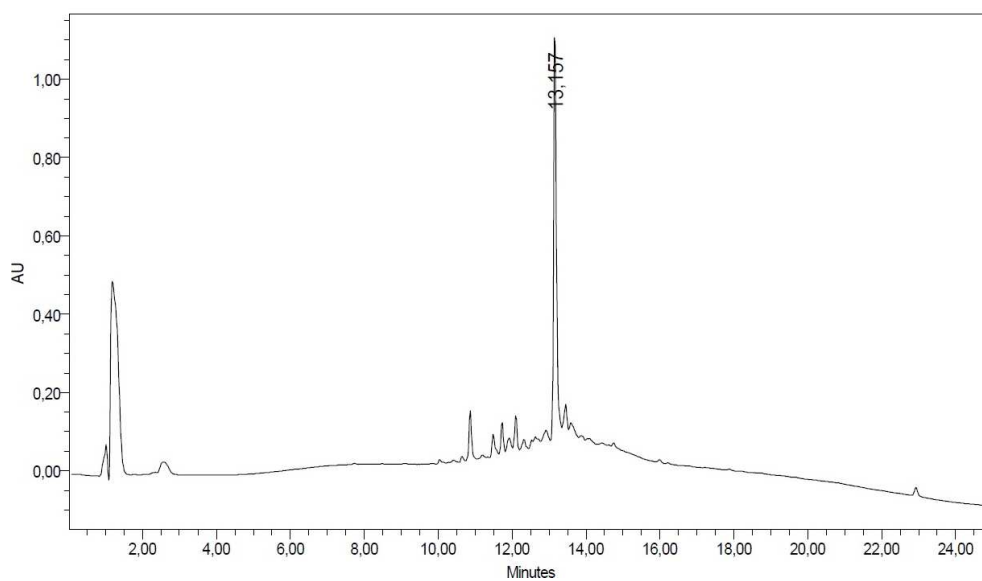


Figure S5: RP-HPLC profile of crude 7.

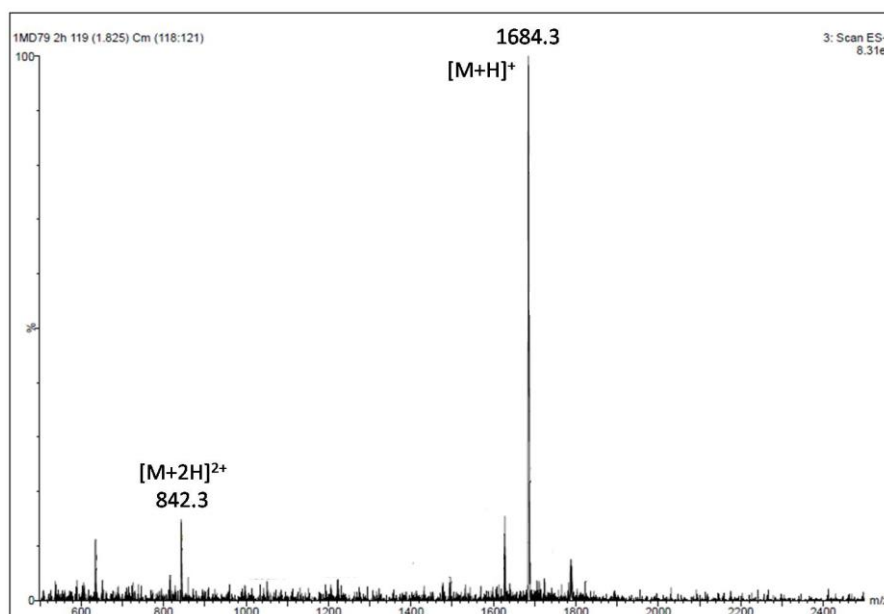
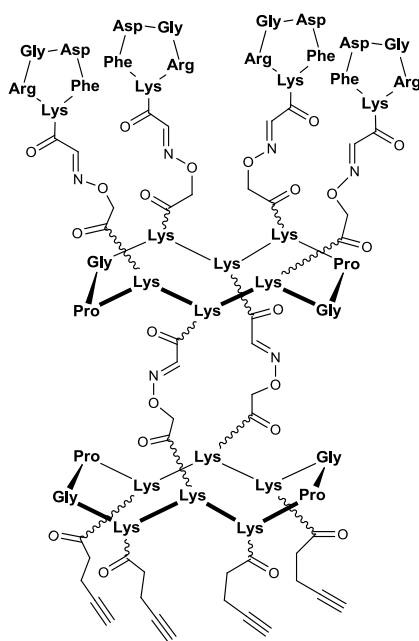


Figure S6: ESI-MS analysis of crude 7.

Mass spectrum (ESI, positive mode) calculated mass for  $C_{82}H_{126}N_{18}O_{20}$ : 1682.9; found: 1683.3.

## 2.4 Conjugate 9



RP-HPLC profile and ESI-MS analysis of 9

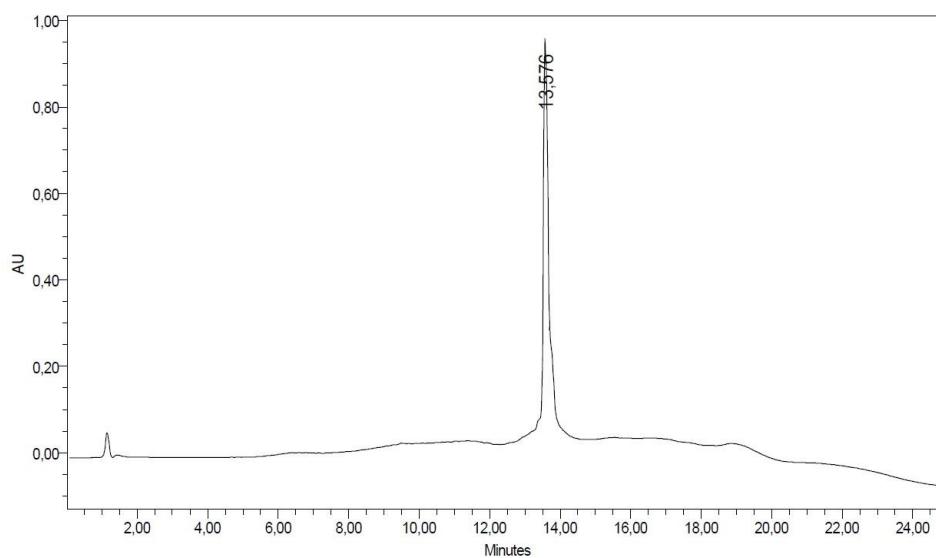


Figure S7: RP-HPLC profile of 9.

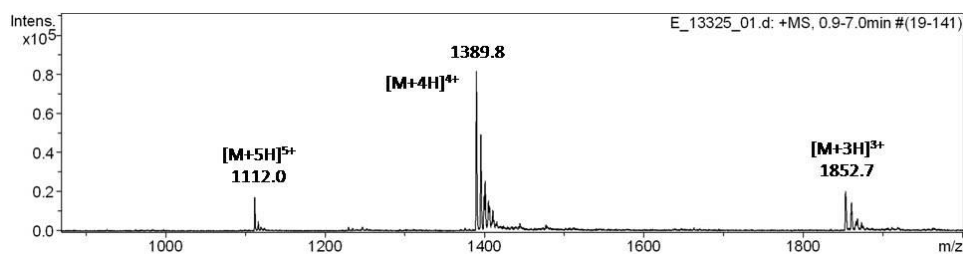
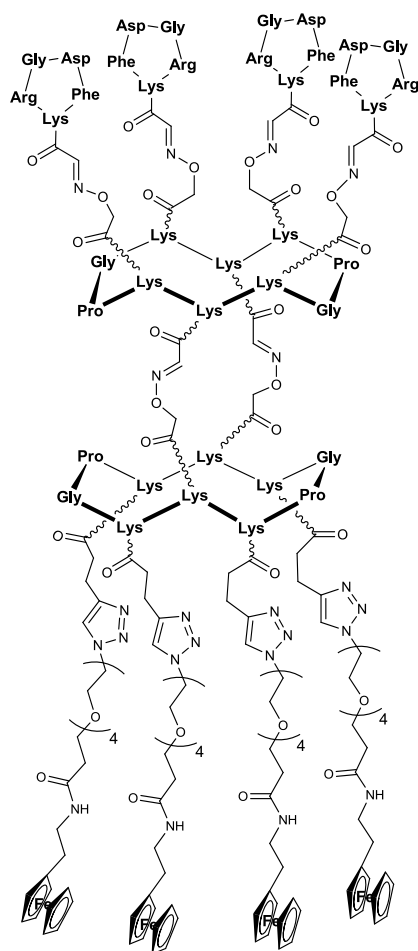


Figure S8: ESI-MS analysis of 9.

Mass spectrum (ESI, positive mode) calculated mass for  $C_{252}H_{370}N_{74}O_{70}$ : 5555.8; found: 5556.2.

## 2.5 Conjugate 1



RP-HPLC profile and ESI-MS analysis of 1

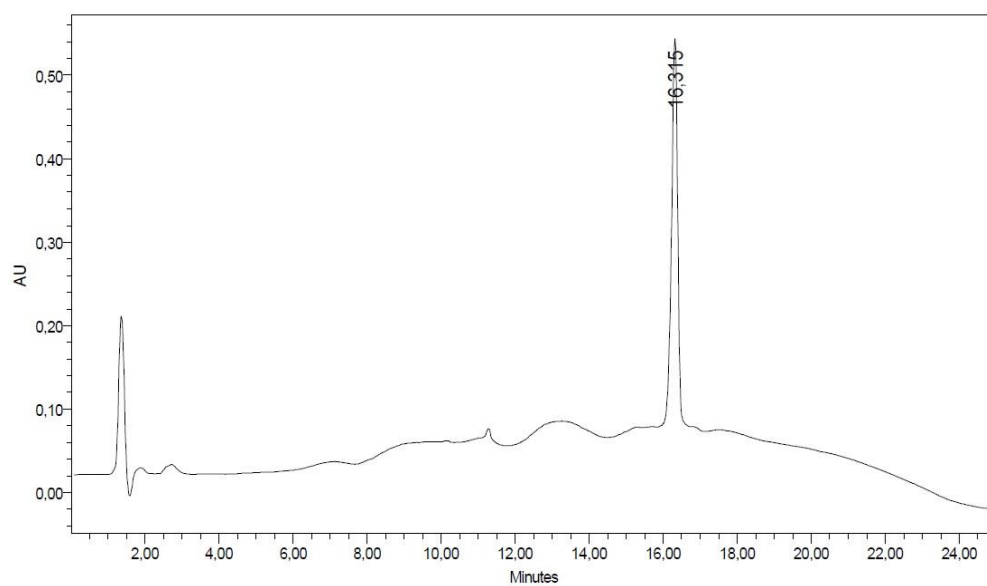
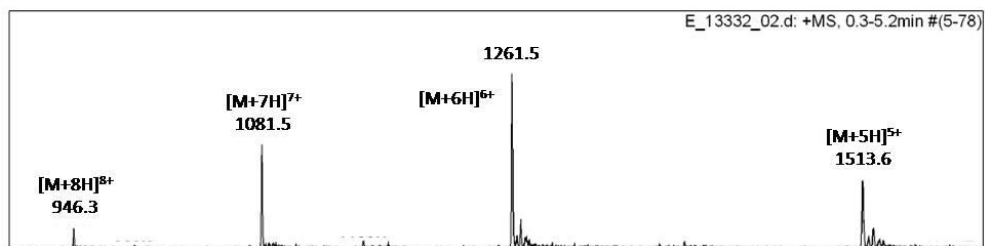


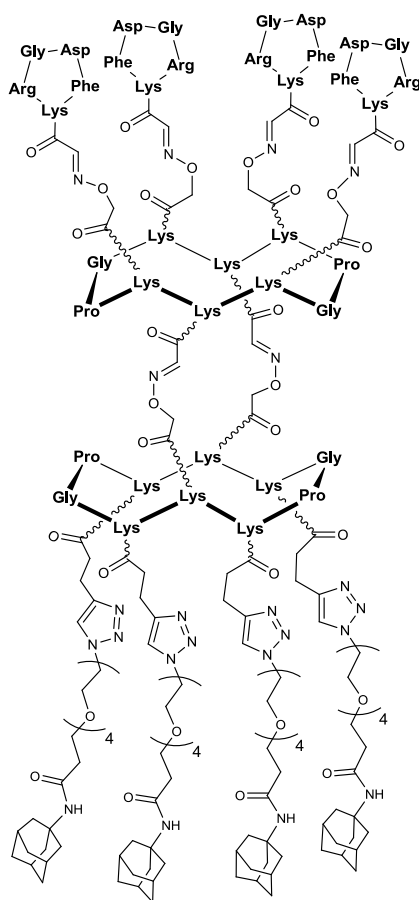
Figure S9: RP-HPLC profile of 1.



**Figure S10:** ESI-MS analysis of **1**.

Mass spectrum (ESI, positive mode) calculated mass for  $C_{344}H_{506}Fe_4N_{90}O_{90}$ : 7565.5; found: 7564.3.

## 2.6 Conjugate 3



### RP-HPLC profile and ESI-MS analysis of 3

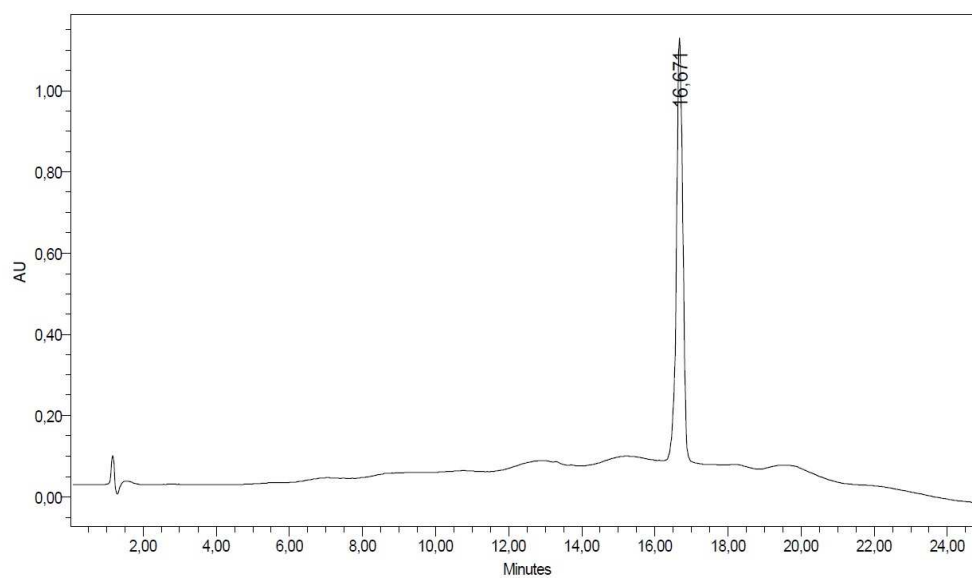
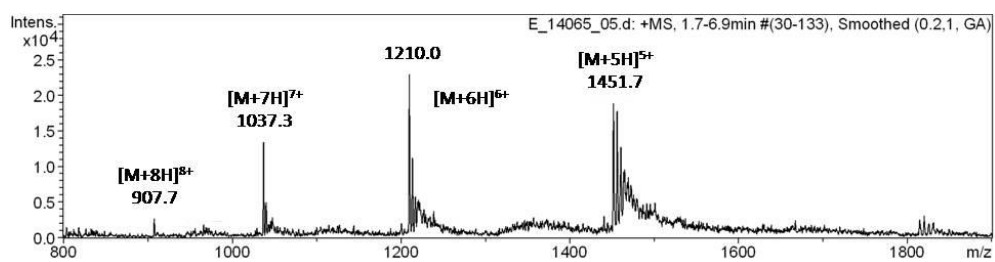


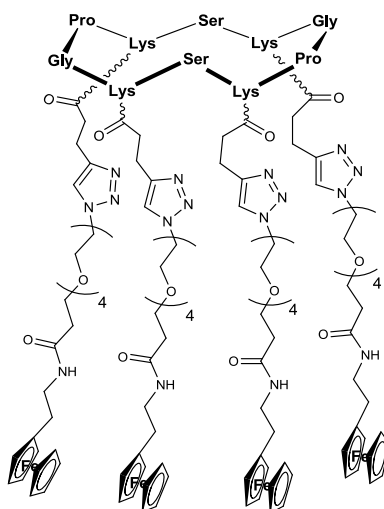
Figure S11: RP-HPLC profile of 3.



**Figure S12:** ESI-MS analysis of **3**.

Mass spectrum (ESI, positive mode) calculated mass for C<sub>336</sub>H<sub>514</sub>N<sub>90</sub>O<sub>90</sub>: 7254.2; found: 7254.8.

## 2.7 Conjugate 4



Compound **4** was prepared according to a strategy described earlier.<sup>1</sup>

### RP-UHPLC profile and ESI-MS analysis of **4**

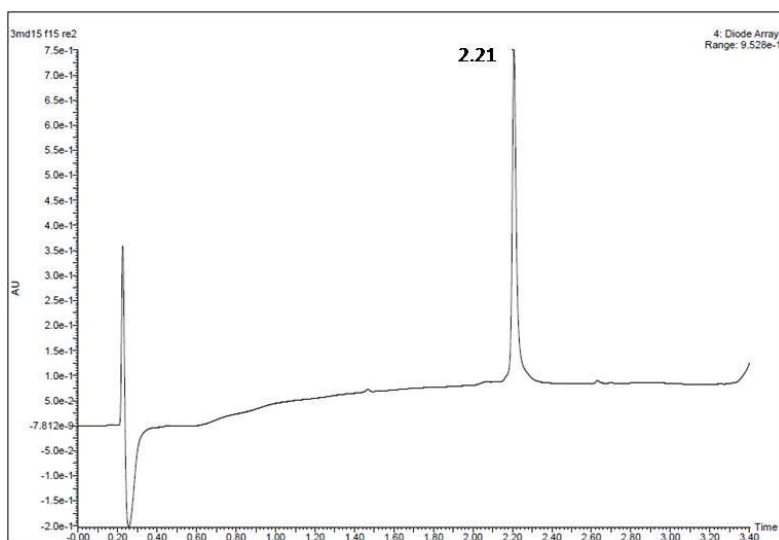


**Figure S13:** RP-UHPLC profile of **4**.

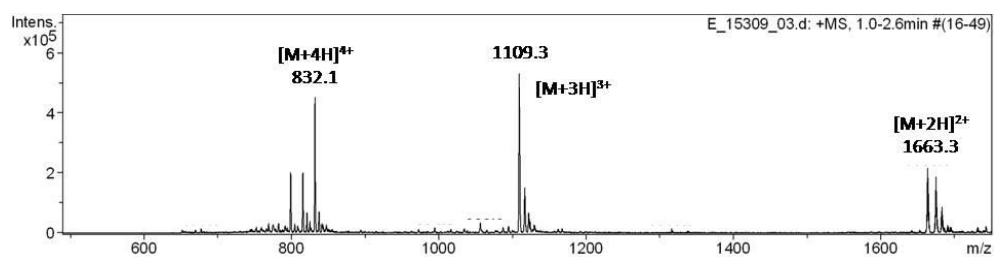


**Figure S14:** ESI-MS analysis of **4**.

Mass spectrum (ESI, positive mode) calculated mass for C<sub>156</sub>H<sub>230</sub>Fe<sub>4</sub>N<sub>30</sub>O<sub>36</sub>: 3324.5; found: 3323.7.

### 3. Supplementary QCM-D data and quantification of adsorbed compound 1, 2 and 4

#### 3.1 Absence of non-specific adsorption of compound 1 on oligoethylene glycol functionalized SAM surface

QCM-D profile presented in the Figure S15 demonstrates the absence of non-specific adsorption of compound **1** on an oligoethylene glycol functionalized SAM surface (prepared by overnight immersion of gold surfaces in pure HS-(CH<sub>2</sub>)<sub>11</sub>-EG<sub>4</sub>-OH at 1mM in ethanol).

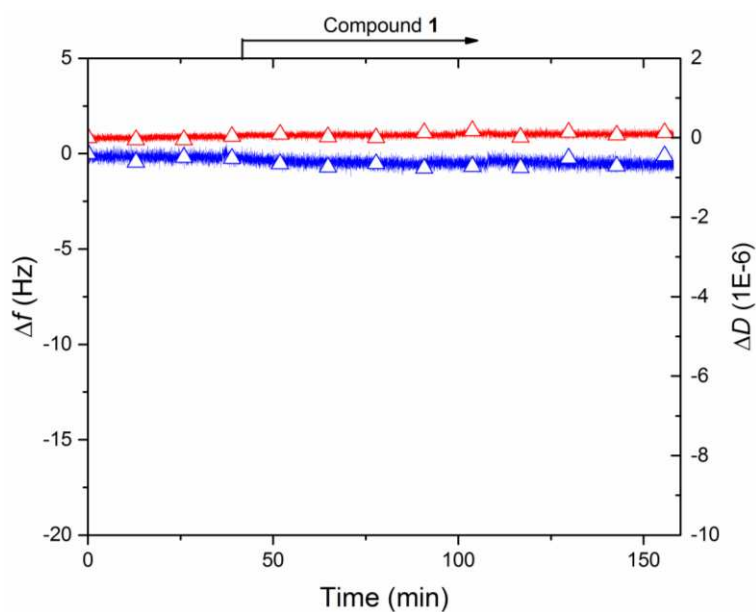


**Figure S15:** QCM-D profile (frequency shift – blue, dissipation shift – red) demonstrating the absence of non-specific adsorption of compound **1** on an oligoethylene glycol functionalized SAM surface lacking  $\beta$ -CD (compound **1** was injected at a concentration of 0.8  $\mu$ M in PBS). Conditions: T = 24°C, flow rate = 20  $\mu$ L.min<sup>-1</sup>. The arrow on top of the graph indicates the start and duration of sample incubation. Before sample incubation, and after saturated binding, the surface was exposed to pure running buffer (PBS).

## 3.2 Quantification of RGD surface densities

### RGD surface densities in mixed peptide derivative monolayers

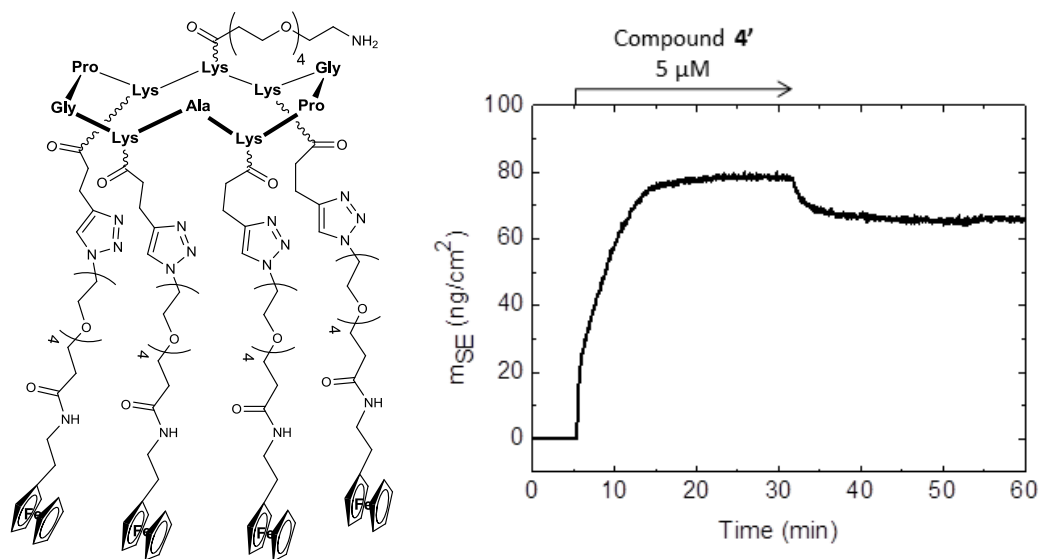


**Figure S16:** Structure and areal mass density of compound **4'** (the structure of this compound is analogous to the compound **4**;  $M = 3773.6$  Da) determined by SE. Start and duration of injection of **4'** ( $5 \mu\text{M}$ ) is indicated by an arrow. Before sample incubation, and after saturated binding, the surface was exposed to pure running buffer (PBS). The surface density of **4'** stably bound after rinsing was  $18.6 \pm 1.0 \text{ pmol}/\text{cm}^2$ .

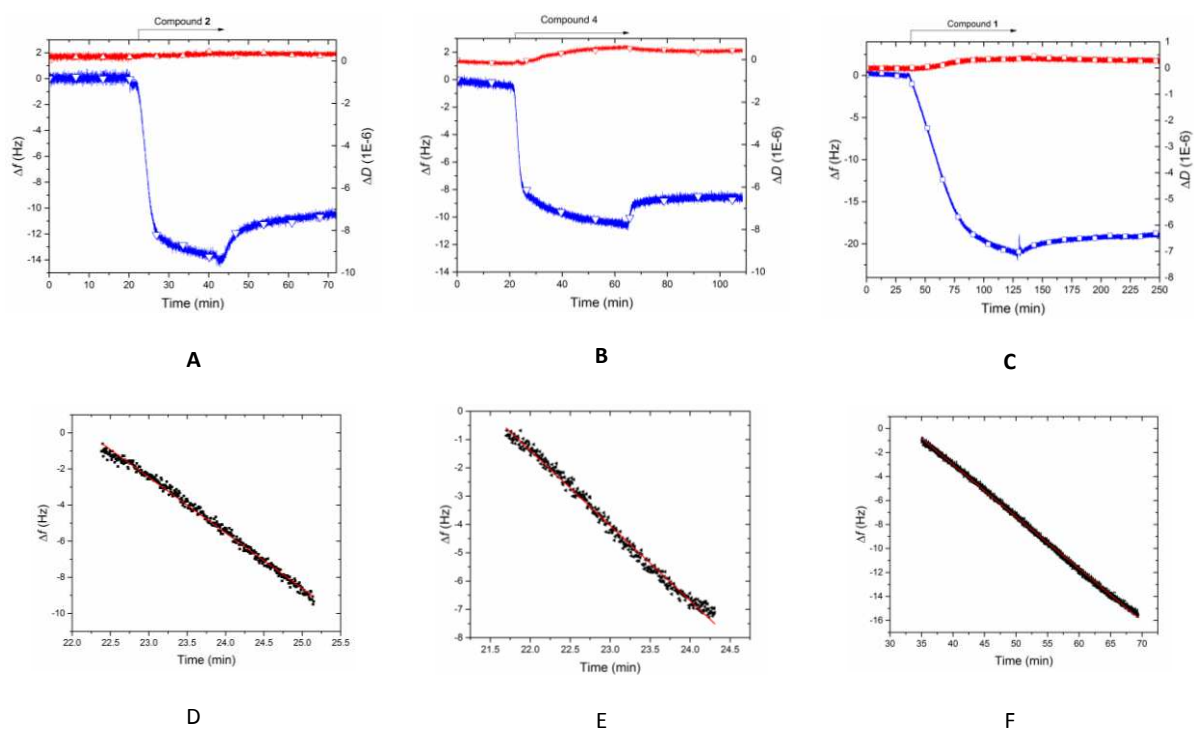


**Figure S17:** (A-C) QCM-D signals (frequency shifts – blue, dissipation shifts – red) recorded during the adsorption of  $3.3 \mu\text{M}$  compound **2** (A) or  $2.5 \mu\text{M}$  compound **4** (B) and  $0.8 \mu\text{M}$  compound **1** (C). The arrows represent the start and duration of sample injections.  $T = 24^\circ\text{C}$ , flow rate =  $20 \mu\text{L}\cdot\text{min}^{-1}$ . (D-F) Linear parts of binding curves (black dots) with linear fits (red lines) for compound **2** (D; data from A), **4** (E; data from B) and **1** (F; data from Figure 3). The frequency response rates  $df/dt$  corresponding to the slopes of the fits are given in Table 1.

#### 4. Optical micrographs of cell adhesion on surfaces displaying compound 1 or 2.

All optical imaging was performed on QCM-D sensors functionalized with  $\beta$ -CD SAM and installed in the Q-Sense Window Module, with 5000 cells/mL injected for 3 min at 100  $\mu$ L/min in DMEM, unless otherwise stated.

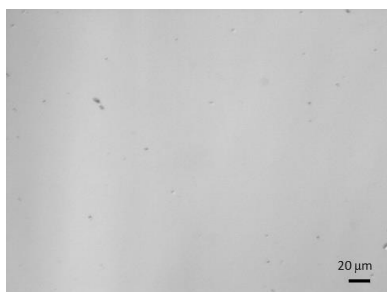


**Figure S18:** HEK-293( $\beta$ 3) cells on 100% compound **4**. No cells are observed, confirming surface passivation. The image is representative of the entire surface.

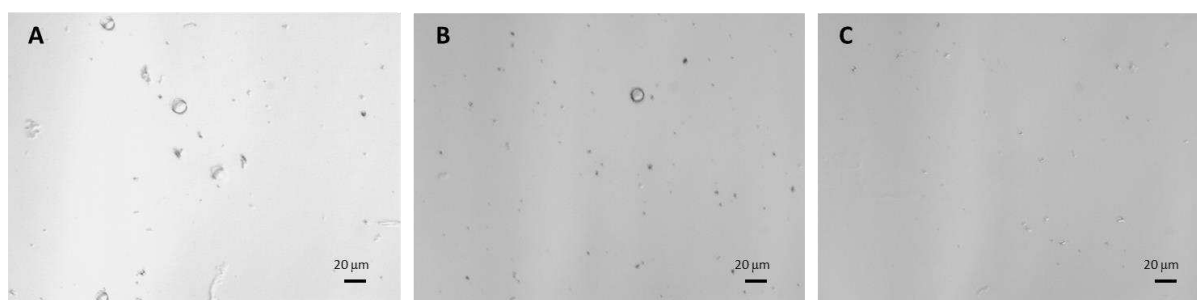


**Figure S19:** (A) HEK-293( $\beta$ 3) cells on 100% compound **1**; (B) HEK-293( $\beta$ 3) cells on 100% compound **2**; (C) HEK-293( $\beta$ 1) cells on 100% compound **1**. The images are representative of the entire surfaces, a few cells per field of view are typically observed.

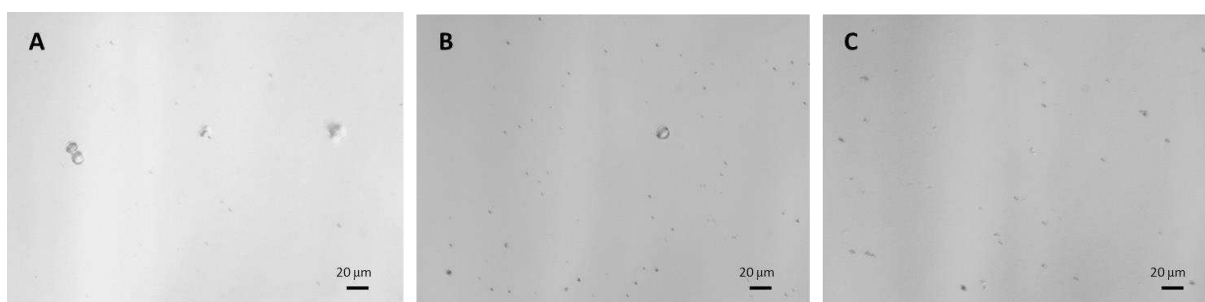


**Figure S20:** (A) HEK-293( $\beta$ 3) cells on 0.95% compound **1**; (B) HEK-293( $\beta$ 3) cells on 1.0% compound **2**; (C) HEK-293( $\beta$ 1) cells on 0.95% compound **1**.

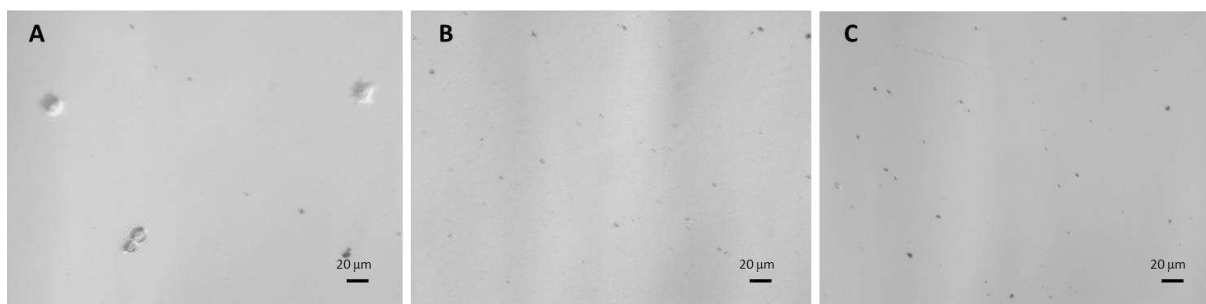


**Figure S21:** (A) HEK-293( $\beta$ 3) cells on 0.084% compound **1**; (B) HEK-293( $\beta$ 3) cells on 0.10% compound **2**; (C) HEK-293( $\beta$ 1) cells on 0.084% compound **1**.

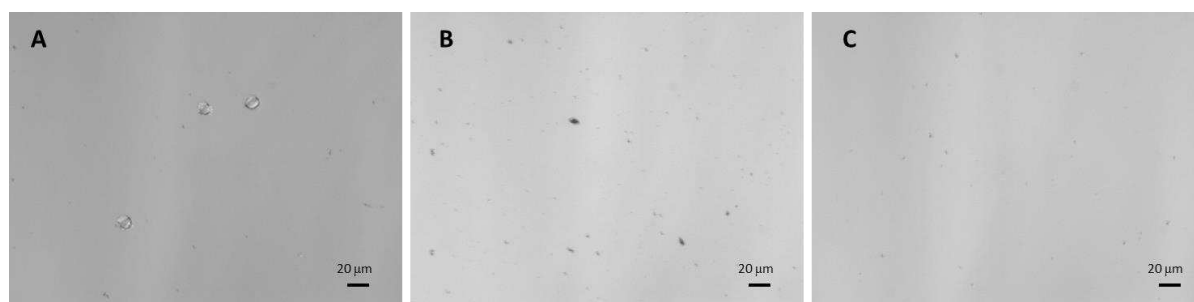


**Figure S22:** (A) HEK-293( $\beta$ 3) cells on 0.0084% compound **1**; (B) HEK-293( $\beta$ 3) cells on 0.00084% compound **1**; (C) HEK-293( $\beta$ 1) cells on 0.0084% compound **1**.

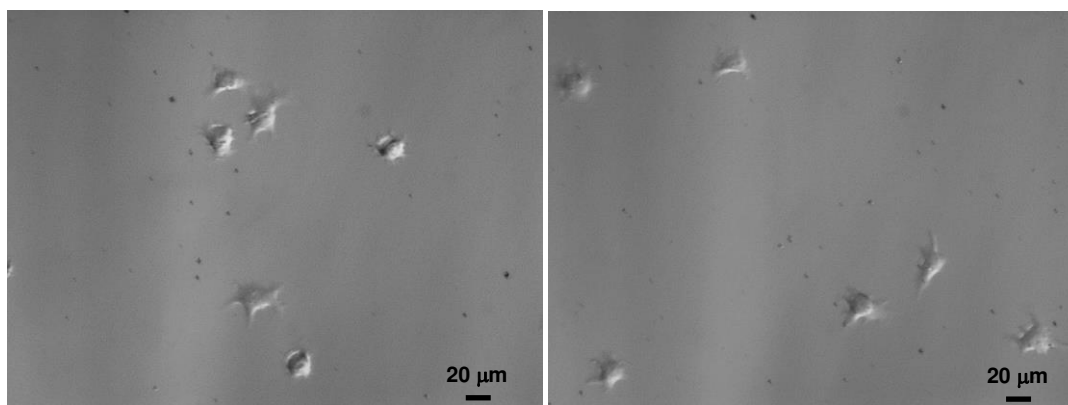


**Figure S23:** HEK-293( $\beta$ 3) cells on 0.0084% compound **1** 20 min after cell injection.

## 5. Electrochemical release of RGD compounds

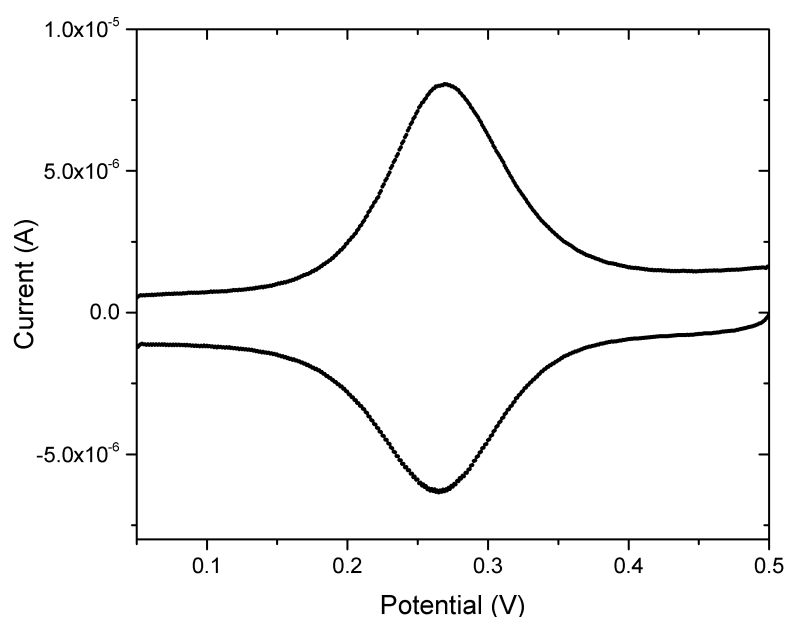


**Figure S24:** Cyclic voltammogram (CV) recorded on gold quartz crystal (QCM-D gold sensor, gold disk diam. 1.1 cm) coated with  $\beta$ -CD SAM functionalized with compound **2** in 0.1 mol.  $L^{-1}$   $KPF_6$  aqueous electrolyte (without compound **2** in solution) ( $\gamma = 100 mV s^{-1}$ ). The CV curve characterized the electrochemical response of Fc encapsulated in  $\beta$ -CD cavity. The observed peak-to-peak potential splitting (5 mV at 100 mV/s) indicates that the voltametric response arises from surface immobilized Fc. We noticed that the reduction peak current (6.3  $\mu A$ ) is lower than the oxidation one (8  $\mu A$ ). This behavior can be explained by the dissociation of the inclusion complex during the Fc oxidation, Fc is converted to  $Fc^{+}$  and the Fc- $\beta$ -CD interaction is broken. Thus, on the reverse sweep less Fc are available for the reduction of  $Fc^{+}$  to Fc (a lower ratio of inclusion complex were restored), because some of Fc compound **2** diffused in the solution. During the time scale of the potential sweep (100 mV/s) the ratio of compound **2** loosed in solution is low. For this electrochemical experiment  $KPF_6$  has been selected because of the lipophilic properties of the  $PF_6^{-}$  anion that facilitates the charge compensation during the electrochemical oxidation of the hydrophobic Fc moieties. In reverse the oxidation of Fc- $\beta$ CD inclusion complex in PBS buffer solution leads to distorted CV curve and the oxidation requires higher potential, that is the reason of 0.55V applied potential.

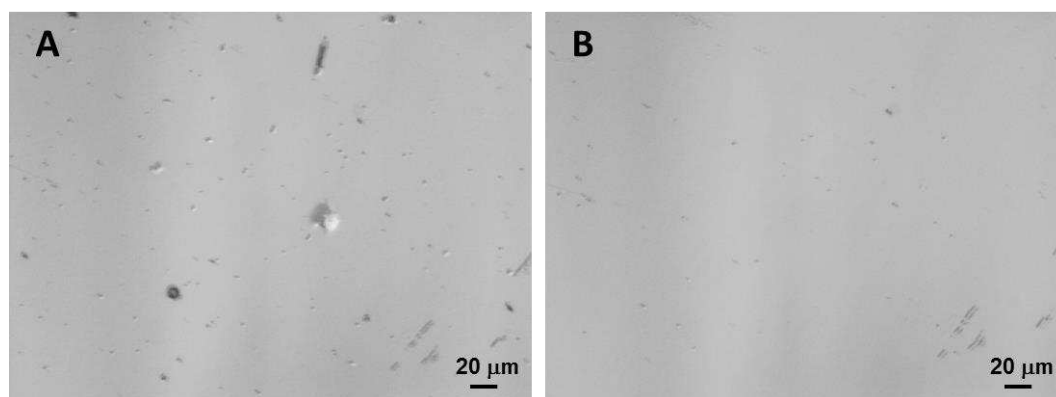


**Figure S25:** Electrochemical detachment assay on HEK-293( $\beta 3$ ) cells on 0.0084% compound **1**. Micrographs (A) was taken after cell injection for 3 min. Micrographs (B) was taken on the same spots after applying an oxidative potential (0.55 V vs. AgCl/Ag), gentle rinsing of the surfaces with DMEM outside the measurement chamber and replacing in the QCM-D module for imaging.

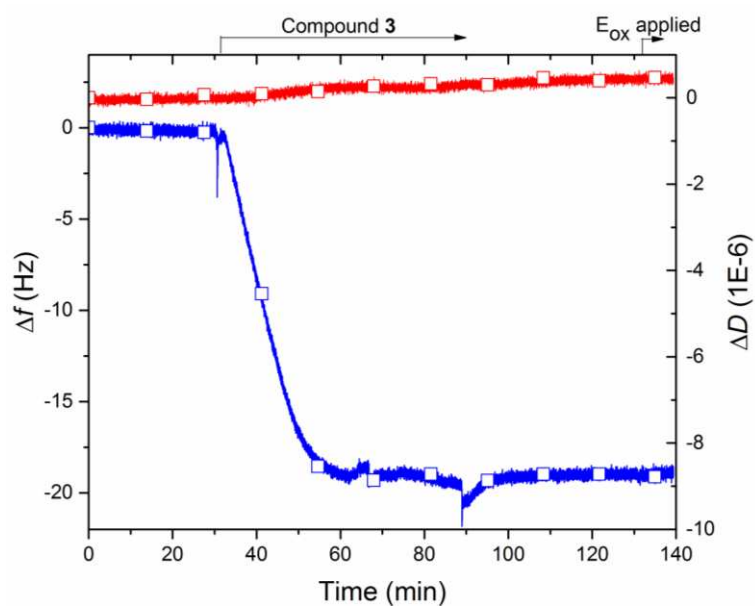


**Figure S26:** Binding of compound **3** ( $2 \mu\text{M}$ ) to a  $\beta\text{-CD}$  SAM and lack of electrochemical release. QCM-D (frequency shifts – blue, dissipation shifts – red) is combined with electrochemistry. Compound **3** is not released by the potential of  $0.55 \text{ V}$  vs.  $\text{AgCl/Ag}$ , confirming that the AD guest layer is not sensitive to the oxidative potential. The arrows represent the start and duration of sample injection and application of oxidative potential;  $T = 24^\circ\text{C}$ , flow rate =  $20 \mu\text{L}\cdot\text{min}^{-1}$ .

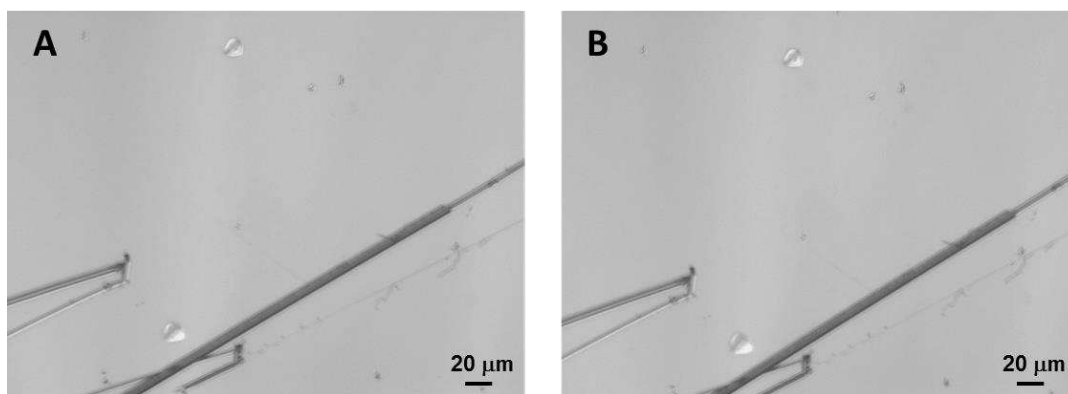


**Figure S27:** Electrochemical detachment assay on HEK-293( $\beta$ 3) cells on 100% compound **3**. Micrograph (A) was taken after cell injection for 3 min. Micrograph (B) was taken on the same spot after the same treatment as for Figures S25B.

## Supplementary reference

---

<sup>i</sup> D. Thakar, L. Coche-Guérente, M. Claron, C. H. F. Wenk, J. Dejeu, P. Dumy, P. Labbé and D. Boturyn, *ChemBioChem* 2014, **15**, 377.

Clustered RGD compounds improve the selective capture and release of cells that express  $\alpha_v\beta_3$  integrin.

